Research Article

Pedogenic carbonate as a transient soil component in a humid, temperate forest (Michigan, USA)

Julia R. Kelson[a,b] (ID), Tyler E. Huth[a,c], Kirsten Andrews[a], Miriam N. Bartleson[a], Thure E. Cerling[d], Lixin Jin[e] (ID), Matthew P. Salinas[a] (ID) and Naomi E. Levin[a] (ID)

[a]Department of Earth and Environmental Sciences, University of Michigan, Ann Arbor, Michigan 48109, USA; [b]Department of Earth and Atmospheric Sciences, Indiana University, Bloomington, Indiana 47405, USA; [c]Department of Earth, Environmental, and Planetary Sciences, Washington University in St. Louis, St. Louis, Missouri 63130, USA; [d]Geology and Geophysics, University of Utah, Salt Lake City, Utah 84112, USA and [e]Department of Earth, Environmental, and Resource Sciences, University of Texas at El Paso, Texas 79968, USA

Abstract

In humid, continental Michigan, we identified pedogenic carbonate in a soil profile developed on glacial drift sediments, as rinds, rhizoliths, and filaments (at depths >50 cm). Given that the climate setting is unusual for pedogenic carbonate, we investigated its formation with environmental monitoring and isotope analyses of carbonate ($\delta^{13}C$, $\delta^{18}O$, Δ_{47}, and ^{14}C) and waters ($\delta^{18}O$ and δ^2H). We found covariation in $\delta^{13}C$ and Δ_{47} amongst the carbonate types (rhizoliths, rinds, filaments, bulk soil, and detrital clasts), and ^{14}C ages of rinds that predate plausible formation ages. The $\delta^{13}C$ and Δ_{47} values of the bulk carbonate and some of the pedogenic morphologies are not fully compatible with pedogenic formation in the modern environment. The $\delta^{18}O$ data from precipitation and river waters and from carbonates are not uniquely identifying; they are compatible with the soil carbonate being pedogenic, detrital, or a mix. We conclude that the soil carbonate is likely a physical mix of pedogenic and detrital carbonate. Pedogenic carbonate is forming in this humid setting, likely because seasonal cycles in soil respiration and temperature cause cycles of dissolution and re-precipitation of detrital and pedogenic carbonate. The pedogenic carbonate may be a transient feature as carbonate-rich till undergoes post-glacial chemical weathering.

Keywords: Inorganic soil carbon, pedogenic carbonate, clumped isotopes, chemical weathering, temperate forests

(Received 2 February 2024; accepted 30 August 2024)

Introduction

Soil carbonate is a significant component of the global carbon cycle, composing 40–50% of total global soil carbon (Eswaran et al., 2000; Plaza et al., 2018). The term "soil inorganic carbon" or "soil carbonate" is used to describe carbonate in soil that is pedogenic, detrital, or biogenic in origin (Monger et al., 2015; Zamanian et al., 2016). Pedogenic carbonate refers to carbonate that precipitates in situ in soil pore water. Detrital carbonate refers to carbonate inherited from parent carbonate material, such as finely ground limestone or dust. Biogenic carbonate forms as animal or plant skeletons (e.g., shells or seeds). Amongst these three forms of soil carbonate, pedogenic carbonate is of particular interest because it represents active fluctuations in the pools of soil inorganic carbon. Furthermore, pedogenic carbonate is commonly used as a paleoclimate archive because its stable isotope composition is related to environmental conditions at the time of its formation (e.g., Cerling and Quade, 1993; Kelson et al., 2020).

Pedogenic carbonate is most commonly found and studied in drylands, where the balance between limited rainfall and high evaporation is thought to promote the accumulation of calcites (e.g., Arkley, 1963; Royer, 1999; Retallack, 2005; Breecker et al., 2009; Slessarev et al., 2016). Though less explored, humid environments host as much as 20% of the global stock of soil carbonate (Plaza et al., 2018; United States Department of Agriculture, Natural Resources Conservation Service, 2022), some of which is interpreted to have a pedogenic origin (Cerling, 1984; Strong et al., 1992; Wang et al., 1993; Railsback, 2021; Licht et al., 2022). An understanding of the origin and the processes driving the formation of pedogenic carbonate in humid environments would therefore help understand the factors that contribute to spatial variation in soil carbonate (Slessarev et al., 2016; Stanbery et al., 2017; Pfeiffer et al., 2023). Understanding the distribution of pedogenic carbonate is important to help inform predictions of how its global distribution might evolve under climate change and anthropogenic management (Nyachoti et al., 2019; Ferdush and Paul, 2021; Naorem et al., 2022; Stanbery et al., 2023; Wani et al., 2023). Furthermore, pedogenic carbonate can be either a net sink or source of carbon to the atmosphere (e.g., Monger et al., 2015; Sharififar et al., 2023). If pedogenic carbonate is precipitating as an intermediate step during lithogenic carbonate weathering, it

may slow the export of dissolved bicarbonate and alter carbon cycling rates (Szramek and Walter, 2004; Williams et al., 2007).

Here we document an occurrence of pedogenic carbonate in glacial drift in the humid continental climate of southern Michigan. Building on prior local work on carbonate weathering in the shallow vadose zone (Jin et al., 2008a, 2008b, 2009), we use environmental monitoring and isotope geochemistry to explore the origin and formation conditions of the soil carbonate at a site in southern Michigan. We infer the processes driving pedogenic carbonate formation at our site, and discuss its implications for paleoclimate reconstructions, regional chemical weathering, and carbon cycling.

Methods

We investigated soil carbonate formation in southern Michigan (USA) using soil stratigraphy, soil monitoring, water isotope analyses, and carbonate isotope analyses. We first describe the site and modern climate. Then we describe sampling, monitoring, and isotope analysis methods.

Site description

The study site is in the Edwin S. George Reserve (hereafter, "the Reserve"), which is a forest preserve maintained by the University of Michigan (UM), located in southern Michigan, USA (Fig. 1) (42°27.44′N, 83°59.87′W WGS84). Southern Michigan has a humid continental climate. Regional precipitation averages 860 mm/year, well above the ~500 mm/year threshold commonly used to delineate where soils contain abundant calcium carbonate (i.e., the Pedocal/Pedalfer boundary) (D'Avello et al., 2019). Each month has >50 mm precipitation, with May through August being the wettest four months and precipitation primarily falling as snow from November through April. The mean annual air temperature is 8.8°C (winter mean = −3.4°C, summer mean = 20.8°C) (Arguez et al., 2012).
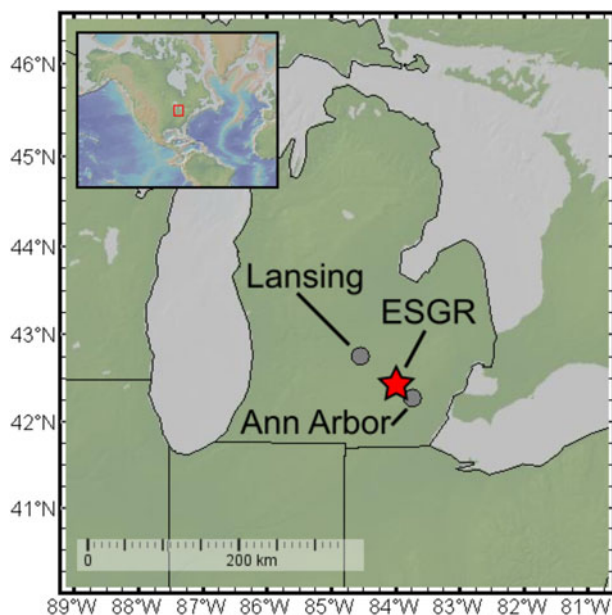

Figure 1. Regional map showing the position of the Edwin S. George Reserve (ESGR) (red star) relative to the cities of Ann Arbor and Lansing, Michigan, with the U.S. state border in black (WGS84 datum used). The inset shows the position of the site in North America.

The geomorphology and topography of the region was strongly influenced by the growth and retreat of the Laurentide Ice Sheet (Dalton et al., 2020), as reflected in sand- and gravel-rich soils, numerous kettle lakes and swamps, and eskers (Rieck, 1976; Farrand and Bell, 1982; Schaetzl, 2001). Glacial sediments are derived from Canadian Shield bedrock and from the sedimentary sequence of Paleozoic and Mesozoic rocks in the Michigan Basin, which include limestones and dolomites (Milstein, 1987; Williams et al., 2007). The glacially reworked sediments in Michigan contain finely ground dolomites and limestones (Schaetzl, 1992; Williams et al., 2007; Jin et al., 2008b), resulting in soil series with mappable amounts of soil carbonate that are a global outlier for their high pH despite the humid climates (Slessarev et al., 2016; United States Department of Agriculture, Natural Resources Conservation Service, 2022). The study site is a knoll about 10 m high that was partially excavated during a gravel quarry operation initiated between 1950 and 1966 (Figs. 2 and 3). Most of the Reserve is forested, including the top of the knoll. The near-vertical, excavated slope itself is unvegetated. The native vegetation of the study site is a mixed oak forest with oak, tamarack, and willow (Roller, 1974; Comer et al., 1995). The forest is dominated by C_3 vegetation: $\delta^{13}C$ values of soil organic matter from the Reserve range from −29.4 to −24.7‰, with an average of −26.8‰ (Jin et al., 2009).

Soil stratigraphy and sample collection

We characterized the Reserve site with soil stratigraphic techniques and monitoring of modern below-ground conditions. We described the stratigraphy in a hand-dug soil pit and in the existing cut slope after we cleared it of vegetation and then further machine-excavated. Field descriptions included depth and thickness of soil and sedimentary horizons, the morphology of clay films, and soil carbonate, grain size, and structure (Birkeland, 1984) (Fig. 3).

We collected soil, sediment, and water samples. The soil and sediment samples included several morphologies of soil carbonate, including rhizoliths, rinds on the bottoms of clasts (<1 mm thick), thin filaments ("stringers"), diffuse carbonate in the soil matrix, bulk sediment (matrix), and limestone/dolostone clasts. We collected water samples from within and outside of the Reserve. Within the Reserve, the soil water and surface water from East Marsh were opportunistically collected (fall 2020 to fall 2022) (n = 12 marsh samples, n = 29 soil water samples collected on 12 unique events). We collected bulk soil for soil water sampling when soil pits were dug for monitoring installation and then subsequently with a hand auger (typical depths of 10, 25, and 50 cm). We extracted the soil water from the bulk soil samples via a custom-built, cryogenic vacuum extraction line at UM (largely following that of West et al., 2006). Outside of the Reserve, we implemented a longer-term precipitation and river monitoring program in nearby Ann Arbor, Michigan (30 km distant, Fig. 1) (started fall 2018, ongoing). Weekly precipitation samples were collected with a no-oil collector (after Gröning et al., 2012). Weekly Huron River samples were initially collected from a dock upstream of the Argo Dam (May–October 2018) and subsequently downstream from the Fuller Street bridge (October 2018 to present, with a hiatus in summer 2020). We collected water and bulk soil samples into vials with polycone seal caps; caps were then wrapped with Parafilm as a secondary barrier to evaporation. We stored the vials upside down at room temperature at UM until analysis.

To further characterize the modern soil system, we monitored soil temperature and soil moisture at depths of 10, 30, and 60 cm and soil CO_2 concentration (pCO_2) at 60 cm (Fig. 4). We
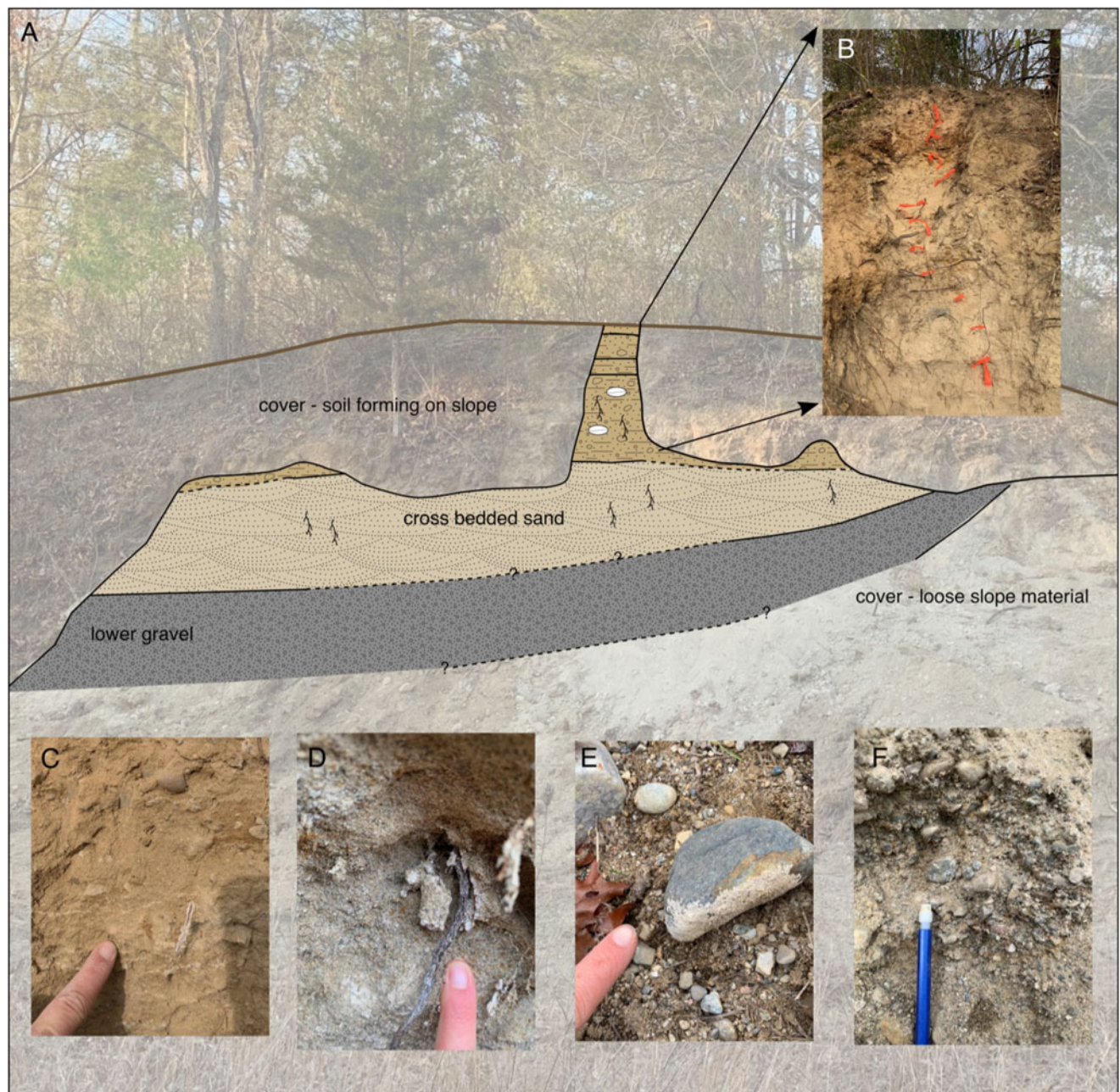
Figure 2. Overview of the study site and soil carbonate morphologies. (A) Photo of the excavated cut slope of the knoll with overlaid interpretational sketch. (B) Photograph of the soil horizons developed on the uppermost gravel unit 9 (see description in Fig. 3). Orange flags are spaced 20 cm apart. (C) Stringer (filaments) and a rhizolith at 90 cm depth. (D) Rhizolith encasing a root at 270 cm depth. (E) Carbonate rind coating a clast. This clast was found in the float at the base of the excavated knoll. Rinds on the undersides of clasts were found in situ at 40 cm and below. (F) Rinds coating clasts and diffuse carbonate in the matrix of the lower gravel unit (depths of 325–400 cm). Pencil for scale.

monitored soil temperature with a HOBO Pendant, soil moisture with a HOBO RX3000 Remote Monitoring Station equipped with HOBOnet Soil Moisture EC-5 Sensors, and soil CO_2 concentration with a CO2meter.com K33 ELG sensor capable of analyzing 0–10,000 ppm CO_2. The monitoring regime covered winter 2021 to winter 2022, with gaps due to equipment failure.

Isotope analytical methods

We analyzed water and carbonate isotope compositions to investigate the conditions of soil carbonate formation.

Water stable isotope analyses

We measured the oxygen and hydrogen ($\delta^{18}O$ and δ^2H) compositions of meteoric and water samples (Fig. 5). All water samples were introduced to instrumentation as liquid water. The $\delta^{18}O$ and δ^2H were measured via Cavity Ring Down Spectrometry primarily at UM and secondarily at Washington University in St Louis (WU). The UM system consists of a Picarro A0325 Autosampler, A0211 Vaporizer, and A0214 Micro-Combustion Module connected to a Picarro L2130-i Analyzer. We normalized the isotope values to the Vienna Standard Mean Ocean Water (VSMOW) scale using four in-house liquid water standards that
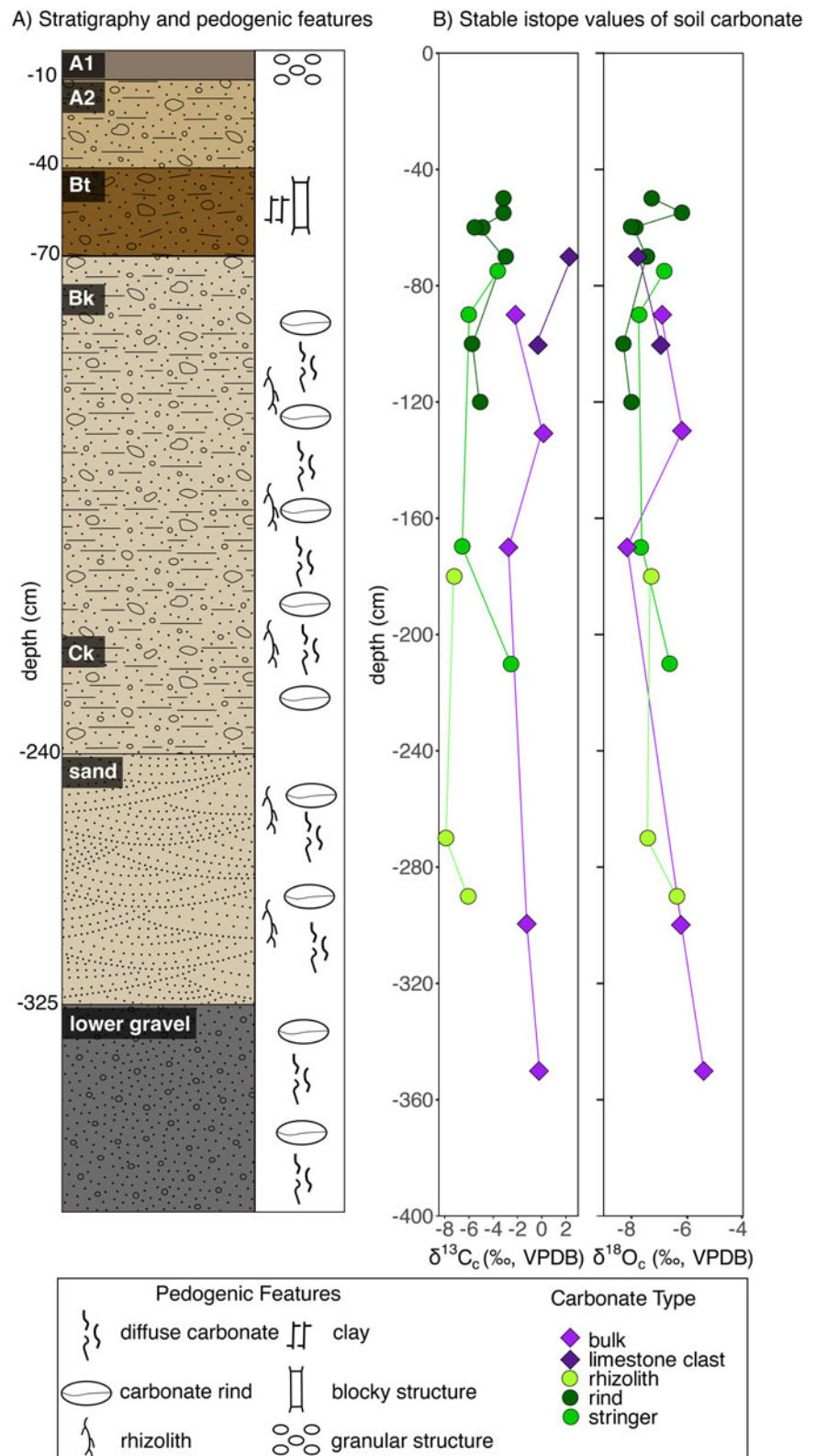
Figure 3. Site stratigraphy and soil carbonate stable isotope values. (A) Sedimentary composition and pedogenic features described on the excavated, cut slope of the knoll. (B) Stable isotope values ($\delta^{13}C$ and $\delta^{18}O$) of soil and detrital carbonate samples that were collected from the excavated slope of the knoll and in soil pits dug from the top of the knoll (depth to carbonate differed by 20–40 cm between those locations). Lines connect data points of the same carbonate type.

are referenced to U.S. Geological Survey (USGS) water standards (USGS45, 46, 49, and 50). Precision is typically better than 0.1‰ in $\delta^{18}O$ and 0.5‰ in δ^2H based on repeat measurements of deionized water (Aron et al., 2020). The WU system consists of a Picarro A0325 Autosampler, A02 Vaporizer, and A0214

Micro-Combustion Module connected to a Picarro L2140-i Analyzer that was run with two lasers activated (i.e., the ^{17}O-mode). We normalized the samples to VSMOW2 and Standard Light Antarctic Precipitation 2 (SLAP2) using in-house liquid waters and international reference waters (Hutchings and
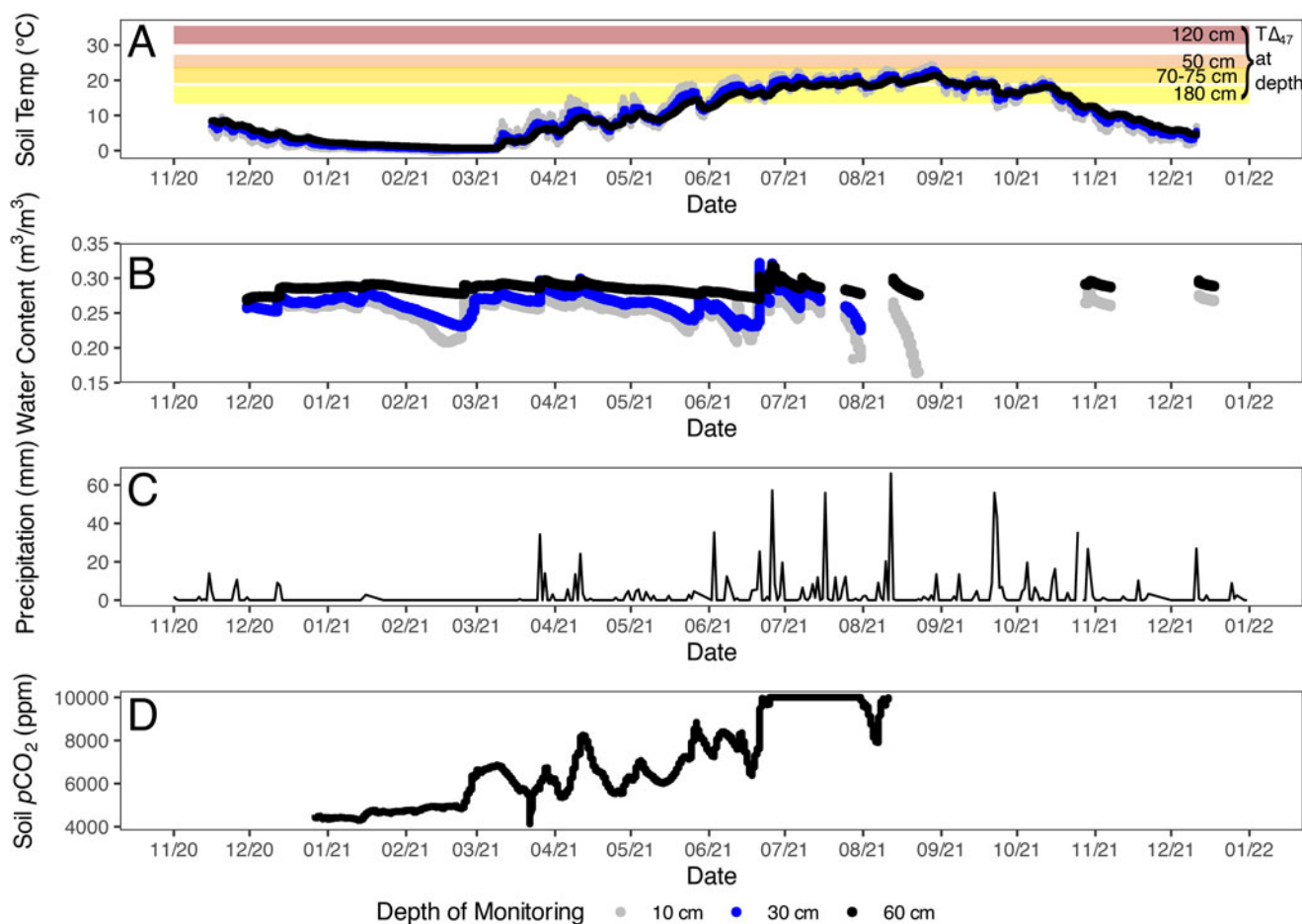
Figure 4. Below-ground soil monitoring data and precipitation data. (A) Soil temperature measured at depths of 10, 30, and 60 cm (lines). Colored horizontal stripes indicate $T\Delta_{47}$ values (±1 SE) for soil carbonate samples with Δ_{47} data (20ESGR-50, 20ESGR-slope-120, 20ESGR-slope-70-75, 22ESGR-rhizolith-180cm). (B) Soil water content at the site. (C) Daily total precipitation from nearby NOAA weather station US1MIWS0055 42.43423, −83.68679), accessed via Climate Data Online on August 18, 2023 (https://www.ncei.noaa.gov/cdo-web/). (D) Soil CO_2 concentrations measured at 60 cm only. The sensor used reaches a maximum at 10,000 ppm; summertime pCO_2 values exceed the maximum.

Konecky, 2023). Typical root-mean-square error (RMSE) of known waters is 0.1‰ in $\delta^{18}O$ and 0.5‰ in δ^2H. For water samples with replicate measurements, typical standard deviations are 0.1‰ in $\delta^{18}O$ and 0.2‰ in δ^2H. We report *d*-excess as a secondary isotope parameter for all water samples (*d*-excess = $\delta^2H - 8 \times \delta^{18}O$).

Carbonate carbon, oxygen, and clumped stable isotope analytical methods

We processed several distinct carbonate morphologies for isotope analysis. We hand-picked gravels from the bulk sediment. For rinds and rhizoliths, we brushed the soil off the outer surface. We then carefully removed the rind material from the parent clast with a hand drill. We homogenized and crushed the cleaned rhizoliths. We hand-picked thin filaments of carbonate ("stringers") out of the soil matrix and then homogenized the material. We cut open limestone/dolostone clasts and then subsampled the cut surface with a hand drill.

We measured carbonate $\delta^{13}C$ and $\delta^{18}O$ (hereafter $\delta^{13}C_c$ and $\delta^{18}O_c$) using a Kiel IV automated preparation device connected online to an isotope ratio mass spectrometer (a Delta V or a ThermoFisher MAT 253) at UM, standardized with NBS-19 to the Vienna Pee Dee Belemnite (VPDB) scale. Typical standard deviations of known values are <0.1‰ for $\delta^{13}C$ and $\delta^{18}O$.

Clumped isotope (Δ_{47}) geochemistry refers to the temperature-dependent clumping between ^{13}C and ^{18}O in a carbonate mineral (Eiler, 2007; Huntington and Petersen, 2023). For Δ_{47} analyses, we prepared samples on a custom, automated vacuum extraction line connected to a Nu Perspective at the Isotopologue Paleosciences Laboratory at UM. First, 6–9 mg of carbonate equivalent of sample material was acidified in a common bath of phosphoric acid held at 90°C. The resulting CO_2 was passed with helium through cryogenic water traps and a Poropak Q column. We calculated the Δ_{47} values using the ^{17}O parameters of Brand et al. (2010) (Daëron et al., 2016; Schauer et al., 2016) and projected them into the ICDES90 reference frame (Bernasconi et al., 2021; Daëron, 2021) using online equilibrated and heated gases (30°C and 1000°C) and carbonate standards ETH1–3. Typically, the standard deviation of Δ_{47} values of each standard is <0.02‰ within a session, and the long-term standard deviation of an in-house standard (102GCAZ01) is 0.014‰. We calculated temperatures (hereafter $T\Delta_{47}$) using the empirical calibration of Anderson et al. (2021) ($\Delta_{47} = 0.0391*10^6/T^2 + 0.154$).

Strontium isotope analyses

We selected two carbonate rind samples for strontium isotope analysis ($^{87}Sr/^{86}Sr$), which was carried out at the University of

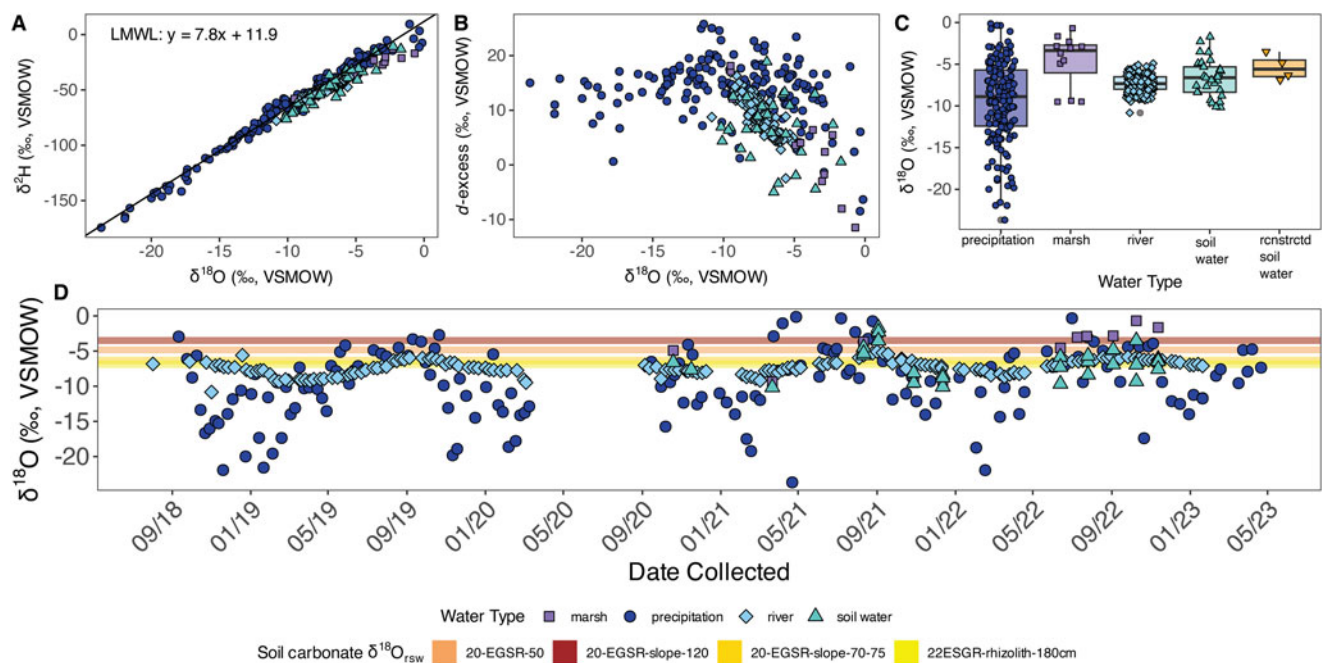**Figure 5.** Stable isotope values ($\delta^{18}O$, $\delta^{2}H$) of surface and soil waters from southern Michigan and reconstructed soil waters ($\delta^{18}O_{rsw}$) from soil carbonates. (A) $\delta^{18}O$–$\delta^{2}H$ relationships for meteoric waters and soil waters. The local meteoric water line (LMWL) is calculated from precipitation data. (B) $\delta^{18}O$–d-excess values for of all water types. (C) Box plots of $\delta^{18}O$ values of water, soil water, and reconstructed soil water. (D) $\delta^{18}O$ throughout the collection period. Horizontal colored stripes (orange, red, gold, yellow) indicate the $\delta^{18}O_{rsw}$ values for soil carbonate samples with $T\Delta_{47}$ data (note that 20ESGR-slope-70-75 [gold] and 22ESGR-rhizolith-180cm [yellow] have overlapping values) and their relationship with warm season meteoric water samples.

Utah's inductively coupled plasma mass spectrometry (ICP-MS) Metals and Strontium Isotope Facility. About 50 mg of ground carbonate was digested in 0.5 mL of concentrated HNO_3 at room temperature and then diluted with Type I grade water. Strontium concentration in acid digest was determined using an external calibration curve prepared from a single element Sr standard (Inorganic Ventures, Christiansburg, VA, USA) in a triple quadrupole ICP-MS (Agilent 8900, Santa Clara, CA, USA). Aliquots from the digests containing 200 ng of Sr were then mixed with concentrated HNO_3 and water to 2 M HNO_3 and purified using an automated system (PrepFAST MC, Elemental Scientific, Omaha, NE, USA). $^{87}Sr/^{86}Sr$ ratios were corrected for mass bias using an exponential law and normalizing to $^{86}Sr/^{88}Sr = 0.1194$ (Steiger and Jäger, 1977). To correct for isobaric interferences (e.g., from ^{87}Rb and ^{86}Kr), ^{85}Rb and ^{83}Kr were simultaneously monitored using the corresponding invariant ratios of $^{87}Rb/^{85}Rb = 0.385706$ and $^{86}Kr/^{83}Kr = 1.502522$ (Steiger and Jäger, 1977). Measurement accuracy was assessed via multiple analyses of standard reference material SRM 987 in each run, with an analyzed value of 0.710297 ± 0.000006 (n = 8; mean ± standard deviation) compared to the certified value of 0.71034 ± 0.00026. Analytical precision (standard error) of $^{87}Sr/^{86}Sr$ for all samples was <0.00001.

Radiocarbon dating
We selected two carbonate rinds from the soil pit (50 and 70–75 cm depth) for radiocarbon analysis; 10 mg of chipped

samples were sent to the University of Arizona's Accelerator Mass Spectrometry Laboratory where CO_2 was extracted and purified, graphitized, and analyzed. We calculated the calibrated radiocarbon ages (cal yr BP) using the CALIB 8.0 software with the IntCal09 calibration curve (Stuiver and Reimer, 1993; Reimer et al., 2009) (Table 1, Supplementary Table S1).

Conceptual models for soil carbonate genesis and predictions for its stable isotope composition

We used previously established relationships between the stable isotopic composition of pedogenic carbonate ($\delta^{13}C$, $\delta^{18}O$, and Δ_{47}) and its formation environment to predict the stable isotope composition of soil carbonate under three scenarios that involve formation in equilibrium with climate conditions at the Reserve (open and closed system) and its mixing with detrital carbonate (Fig. 6). We employed a simple mixing model to explore the possibility that the soil carbonate is pedogenic carbonate mixed with detrital carbonate particles (Amundson et al., 1988; West et al., 1988a; Kraimer and Monger, 2009; Zhou and Chafetz, 2010; Michel et al., 2013) (Fig. 6A). We modeled linear mixing in $\delta^{18}O$–$\delta^{13}C$ and $\delta^{13}C$–Δ_{47} between various potential endmembers and with a varying fraction of pedogenic carbonates (F) in a Monte Carlo framework (Fig. 7). An example mixing line is shown in Figure 6 (schematically in A and B, calculated in G and H). In the Monte Carlo mixing framework (Fig. 7), we allowed for a range of endmember compositions (Supplementary Code).

Table 1. Radiocarbon and strontium isotope data for soil carbonates from the Reserve.

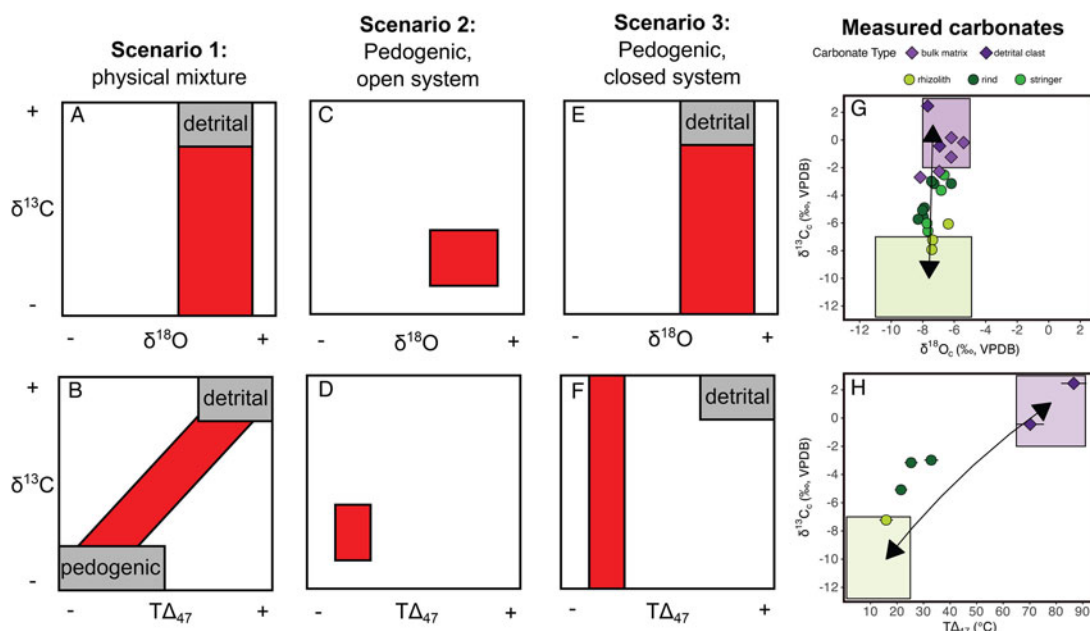| Sample ID	Carbonate morphology	Median ^{14}C ages calibrated using Calib. Rev. 8	^{14}C age error (1-sigma, yr BP)	$^{87}Sr/^{86}Sr$
20ESGR-50cm	rind	23,691 cal yr BP	100	0.709693
20ESGR-70-75cm	rind	17,366 cal yr BP	79	0.709461

Figure 6. Expected and measured isotope patterns for three scenarios explaining the origin of the soil carbonate. Scenario 1 (A and B): A physical mixture between pedogenic and detrital carbonate. In this scenario, $\delta^{13}C$ and $T\Delta_{47}$ vary with the fraction of detrital material. $\delta^{18}O$ is uniform because the $\delta^{18}O$ of carbonate formed in equilibrium with meteoric waters is similar to (within 1–2‰ of) the $\delta^{18}O$ values of detrital carbonates. Scenario 2 (C and D): Pedogenic carbonate in an open system. In this scenario, soil carbonate has a relatively small range of $\delta^{18}O$, $\delta^{13}C$, and $T\Delta_{47}$ values that reflects isotopic equilibrium with the environment during a single season. Scenario 3 (E and F): Pedogenic carbonate in a closed system with respect to soil CO_2. In this scenario, $\delta^{13}C$ varies while $\delta^{18}O$ and $T\Delta_{47}$ are constant. Measured stable isotope values of the distinct carbonate types from the Reserve (G and H). One example of a mixing line calculated between a set of potential pedogenic and detrital endmembers is shown with black lines and arrows (i.e., one iteration of scenario A). Possible ranges of pedogenic and detrital endmember compositions at the Reserve are shown as rectangles outlined in black, filled in green and purple, respectively. These ranges are only illustrative and differ from the ranges used to constrain the mixing model shown (Fig. 8). The illustrated possible ranges of the pedogenic endmember $\delta^{13}C$ values are calculated based on $\delta^{13}C$–CO_2 values measured in the Huron River watershed (Jin et al., 2009). The illustrated range of the pedogenic endmember $\delta^{18}O$ values is based on Huron River waters and a carbonate growth temperature of 15°C. The possible range in $\delta^{18}O$ and $\delta^{13}C$ values of the limestone endmember is based on secular trends from Vezier et al. (1999) and measured limestone clast values. Where error bars are not visible, they are smaller than symbol size. The slight curvature in the $\delta^{13}C$–$T\Delta_{47}$ mixing line is due to nonlinearity in the relationship between temperature and Δ_{47}.

We allowed a range in detrital endmember compositions that was informed by the measured isotopic composition of limestone clasts at the site and the secular isotopic trends through the Phanerozoic (Veizer et al., 1999): $-8 \leq \delta^{18}O \leq -5$, $-2 \leq \delta^{13}C \leq +3$‰, and $0.448 \leq \Delta_{47} \leq 0.495$‰ ($65 \leq T\Delta_{47} \leq 91$°C). For the pedogenic carbonate endmember, we allowed for a wide potential range of compositions that could be reasonably found for the vast majority of pedogenic carbonates found globally: $-15 \leq \delta^{18}O \leq -5$‰, $-14 \leq \delta^{13}C \leq 0$‰, $0.594 \leq \Delta_{47} \leq 0.678$‰ ($0 \leq T\Delta_{47} \leq 25$°C) (e.g., Cerling, 1984; Kelson et al., 2020). Δ_{47} does not mix linearly, but the effect of nonlinearity in our range of values is ~0.0002‰ in Δ_{47} (White and Defliese, 2023), which is much smaller than our external precision in Δ_{47} (the long-term standard deviation of our in-house standard, 102GCAZ01, is 0.014‰). Note, however, that there is nonlinearity between temperature and Δ_{47}; we perform the mixing calculations in Δ_{47} and then calculate temperature. We only used samples with $\delta^{13}C$, $\delta^{18}O$, and Δ_{47} data, and the feasible endmembers for each sample were those capable of reproducing the observed isotope composition within analytical error for all three isotopes (i.e., ±0.1‰ for $\delta^{13}C$/$\delta^{18}O$, ±5°C for $T\Delta_{47}$). For visual clarity we calculated F values in increments of 0.1 and emphasize differences between increments by plotting their average values.

In a canonical calcic soil system, the soil pore water and CO_2 are open to isotopic exchange with incoming meteoric waters and the soil gas reservoir, resulting in a relatively small range in pedogenic carbonate isotope values that reflect formation in equilibrium with soil climate conditions (Fig. 6B) (Cerling, 1984; Cerling

and Quade, 1993; Quade et al., 2013). To model the pedogenic carbonate system, we first calculated the $\delta^{18}O$ values of the carbonate-parent water (i.e., reconstructed soil water, $\delta^{18}O_{rsw}$) using the temperature-dependent isotope fractionation factor informed by $T\Delta_{47}$ data (Kim and O'Neil, 1997) (Fig. 5C). For samples without $T\Delta_{47}$ data, we used the average $T\Delta_{47}$ value to calculate $\delta^{18}O_{rsw}$. Choice of calibration for the fractionation factor does not materially change our interpretations (i.e., Coplen, 2007 vs. Kim and O'Neil, 1997). We compared the $\delta^{18}O_{rsw}$ to measured $\delta^{18}O$ values of meteoric and soil waters.

Then, we modeled the set of environmental conditions potentially capable of producing the measured soil carbonate $\delta^{13}C$ values using established equations that relate pedogenic carbonate to soil respiration, the overlying vegetation, and the atmosphere. For each sample, we first calculated the $\delta^{13}C$ of soil gas ($\delta^{13}C_s$) from the measured $\delta^{13}C$ of soil carbonate ($\delta^{13}C_c$) and its formation temperature (Romanek et al., 1992):

$$\varepsilon_{cl\text{-}CO_2} = 11.98 - 0.12 * T \qquad (1)$$

where $\varepsilon_{cl\text{-}CO2}$ is the mineral-gas fractionation factor for calcite (i.e., $\delta^{13}C_s = (\delta^{13}C_c + 1000)/(\varepsilon_{cl\text{-}CO_2}/1000 + 1) - 1000$). Then, we modeled the $\delta^{13}C$ of soil respiration ($\delta^{13}C_r$) (Cerling, 1984; Cerling and Quade, 1993; Davidson, 1995):

$$\delta^{13}C_r = (\delta^{13}C_s - 4.4 - C_a/C_s * \delta^{13}C_a + 4.4 * C_a/C_s)$$
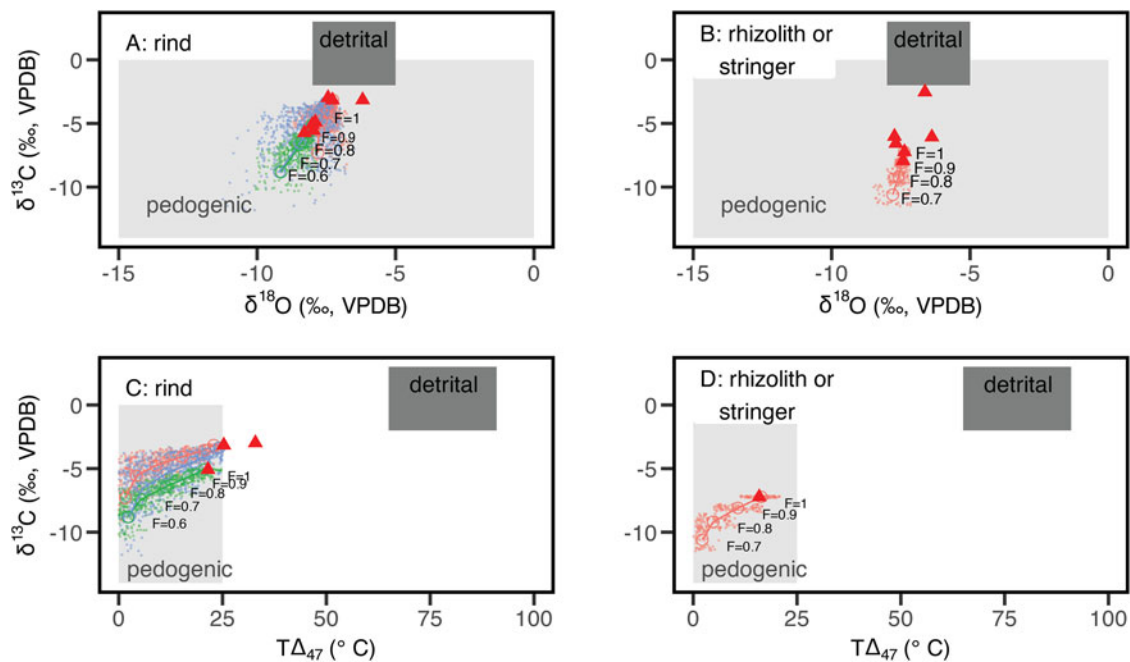$$/(1.0044 - C_a/C_s * 1.0044) \qquad (2)$$

Figure 7. Solutions for the model of two-component mixing between detrital and pedogenic carbonate. Plots show solutions for carbonate in sample groups separated as rinds (A and C) and rhizoliths or stringers (B and D) in $\delta^{13}C$–$\delta^{18}O$ and $\delta^{13}C$–$T\Delta_{47}$ space. We only modeled samples with $\delta^{13}C$, $\delta^{18}O$, and Δ_{47} data to provide maximum constraint on solutions for F. The dark gray box outlines the possible detrital endmember values, the light gray box outlines the full range of possible pedogenic carbonate endmember values on a global basis, and the red triangles are observed sample values. The small colored dots are the feasible pedogenic carbonate endmembers that can mix with the detrital endmember to create the observed soil carbonate isotope composition at the assigned fraction of pedogenic carbonate (F). Different colors denote mixing model solutions for different samples. For visual clarity, we show simulations in 10% increments of the fraction of pedogenic carbonate; the large circles are averages for each increment and lines connect the average values. The set of endmember solutions for the assumed fraction of pedogenic carbonate are only labeled for the bottom right sample in each panel (e.g., "solutions for $F = 0.6$"), but all samples have the same pattern. Note that when the assumed fraction of pedogenic carbonate is 100% ($F = 1$), the endmember solutions necessarily match the observed sample isotope composition.

where C_a is atmospheric pCO_2 and C_s is soil pCO_2. This equation is solved independently for each measured $\delta^{13}C_c$ value, each representing a specific depth. The calculations were performed 10,000 times, assuming varying conditions within a plausible range for the Late Quaternary (atmospheric CO_2 concentration: 180 to 280 ppm, soil CO_2 concentration: atmospheric concentration to 10,000 ppm; soil temperature: 0 to 25°C; $\delta^{13}C$ of atmospheric CO_2: −6 to −7‰) (Cerling, 1984; Davidson, 1995; Bereiter et al., 2015; Eggleston et al., 2016; Huth et al., 2020) (Supplementary Code). The modeled conditions that were required to produce the measured $\delta^{13}C_c$ values were then compared to modern conditions (Fig. 8).

Results

Soil profile developed in carbonate-rich glacial drift

We documented a soil profile developed in stratified glacial drift. The soil profile is about 2.4 m thick and consists of two A horizons, a Bt horizon, and a Bk horizon (Figs. 2 and 3). The parent material is fine–medium, poorly sorted sand with 10−15% gravel; evidence of primary sedimentary bedding was not identified. Soil horizons (A1, A2, Bt, Bk, and Ck) were differentiated based on organic content, color, pedogenic structure, and secondary mineral composition (Fig. 3). Notably, the Bk horizon was identified based on the presence of carbonate (i.e., the first depth at which the matrix reacted vigorously with hydrochloric acid application) and the sharp color change relative to the overlying layer. Within the Bk horizon, carbonate was found as stage

I–II rinds on the bottom of clasts, rhizoliths (some surrounding still-intact roots), stringers, and as diffuse fine-grained material within the matrix (Fig. 2). The depth to the Bk horizon varied by up to 50 cm at several sampled locations (instrumented soil pit, auger collections, and the excavated slope) and at other test pits in glacial drift in the region; this variation could be partially due to alteration of the ground surface elevation during historical quarry operations and/or natural variation in leaching depths.

Below the soil profile, we found stratified sands and gravels consistent with a fluvio-glacial drift deposit, such as a kame or an esker (Fig. 3). A layer of cross-bedded sand appears at 2.4 m below the surface. The sand unit is very fine to very coarse and well rounded, with some grain-size separation in the beds. There were abundant carbonate rhizoliths throughout the sand unit, and the matrix reacted vigorously with hydrochloric acid. The gravel unit 3.2 m below the ground surface consisted of lenses of sorted sediments, ranging from rounded–subrounded gravels to medium sand. The gravel unit reacted with HCl vigorously throughout, and many of the clasts displayed incipient (stage I) carbonate rinds (Figs. 2 and 3).

Calcite mineralogy was confirmed with X-ray diffraction analysis of rind material drilled from clasts collected at depths of 50 and 70 cm in a soil pit adjacent to the slope. The $^{87}Sr/^{86}Sr$ values of ≈0.709 for the rinds collected at 50 cm and 70–75 cm are consistent with marine limestone as the parent material (Table 1). The radiocarbon ages are 23,691 cal yr BP and 17,366 cal yr BP for the same rinds collected at 50 cm and 70–75 cm (Table 1).
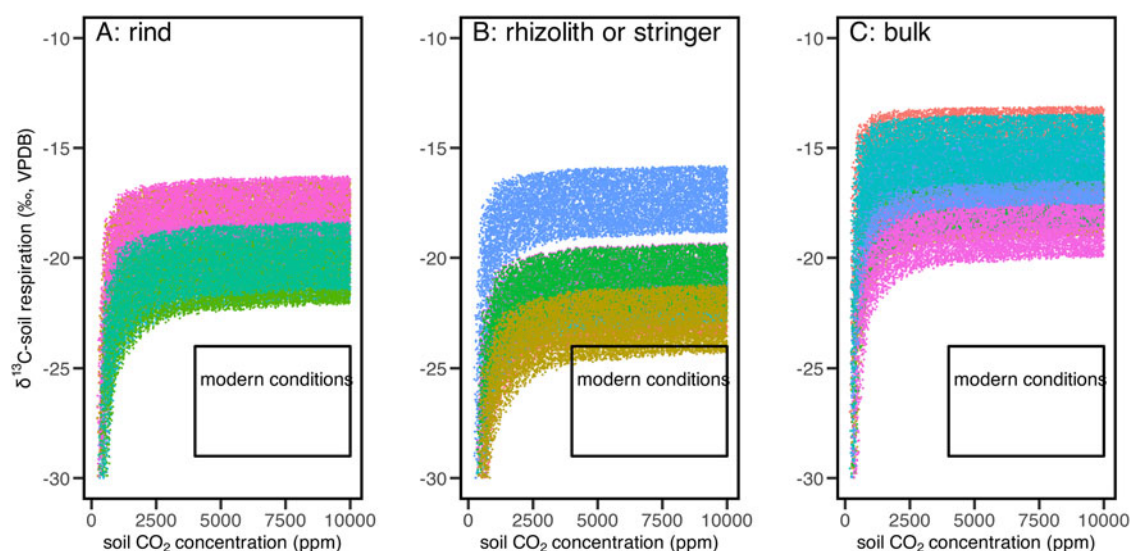
Figure 8. Environmental conditions capable of creating observed soil carbonate $\delta^{13}C$ values assuming samples are pedogenic carbonate formed in an open system. Theoretically feasible conditions for the $\delta^{13}C$ of soil respiration and soil CO_2 concentration are shown for three sample groups: (A) rinds, (B) rhizoliths and stringers, and (C) bulk soil samples. Colored dots denote solution spaces (10,000 iterations each) for different samples. Solutions that are consistent with modern conditions must fall within the black box, which outlines modern conditions for $\delta^{13}C$ of soil respiration in a C_3 dominated landscape (Tipple and Pagani, 2007; Jin et al., 2009) and the observed soil CO_2 concentrations during our monitoring period.

Results of below-ground soil monitoring

Over the year of monitoring we conducted, we observed seasonal cycles in soil temperature, water content, and pCO_2. At carbonate-relevant depths of 60 cm, winter temperatures are near-freezing in January and February (0.6°C). The soil begins to thaw in mid-March, and temperatures reach a maximum temperature of 21.4°C in late August (Fig. 4). Soil water content remains at 0.2–0.3 m^3/m^3 for winter and spring (December through June), with minor fluctuations due to infiltration of snowmelt and precipitation. Initial snowmelt occurred in late February, causing an increase in water content at all depths that was followed by several cycles of increasing and decreasing soil moisture heading into the summer (Fig. 4). The soil pCO_2 values were between 4300 and 4500 ppm midwinter (January to February). In late March, pCO_2 concentrations started to rise above winter lows, and then remained >5000 ppm with spikes of >8000 ppm through early summer. Mid-late summer pCO_2 values (July to August) exceeded 10,000 ppm (the limit of our sensor). The pCO_2 record ended on August 11, 2021. Even considering the relatively short period of monitoring, these data capture the major seasonal trends (Fig. 4).

Results of stable isotope analyses of carbonates and water and of predictions for pedogenic carbonate

The $\delta^{13}C_c$ values of all carbonates are −7.9 to 2.5‰ (VPDB), spanning a 10.4‰ range (Table 2, Figs. 3 and 8). The $\delta^{13}C_c$ values of the rhizolith, stringer, and rind samples are generally lower than those of the bulk matrix and parent limestone clasts (Figs. 3 and 6). The $\delta^{18}O_c$ values of all carbonates are −8.3 to −5.4‰ (VPDB), spanning a 2.9‰ range (Table 2, Figs. 3, 6, and 8). There are not marked differences in $\delta^{18}O_c$ values amongst carbonate morphologies (Fig. 6). A subset of the samples was measured for Δ_{47}, and those values range from 0.4562 to 0.6219‰ (ICDES-90), corresponding to temperatures ($T\Delta_{47}$) of 87 to 16°C (Table 3). The $T\Delta_{47}$ values of the measured rinds and rhizoliths are lower than the $T\Delta_{47}$ values of the limestone clasts (range of

15.9–32.9°C vs. 70.2–86.6°C) (Table 3). There is significant covariation between $\delta^{13}C_c$ and $T\Delta_{47}$ ($r^2 = 0.89$, $P = 0.004$) amongst all the carbonate morphologies, but there is not covariation between $\delta^{18}O_c$ and $\delta^{13}C_c$ or $T\Delta_{47}$ (Fig. 6D).

We observed seasonal variation in the isotopic values ($\delta^{18}O$, δ^2H, and d-excess) of meteoric waters (Fig. 5), typical of continental locations with seasonal fluctuations in air temperature (Rozanski, 1993). There is covariation between $\delta^{18}O$ and d-excess for samples with $\delta^{18}O > \sim-10$‰, indicative of evaporation. The local meteoric water line (i.e., $\delta^{18}O$–δ^2H linear regression) defined by precipitation has a slope of 7.8 that is close to the canonical value of 8 (Table 4) (Putman et al., 2019). The isotopic composition of the precipitation is quite variable ($\delta^{18}O$ ranges from −23.6 to −0.14‰ VSMOW; d-excess ranges from −8.5 to 25.8‰), though the isotopically light precipitation events tend to occur only in the winter and the isotopically heaviest rain occurs in the summer. The Huron River water has less variability in $\delta^{18}O$ and δ^2H than precipitation, but does have a sinusoidal pattern of seasonal variation (Fig. 5), with low $\delta^{18}O$ values (high d-excess values) in the winter (typical minimum $\delta^{18}O$ of −9 ‰ and maximum d-excess of +15) and high $\delta^{18}O$ values (low d-excess values) in the summer (typical maximum $\delta^{18}O$ of −5 and minimum d-excess of +5) (Pelletier, 2020). East Marsh in the Reserve has $\delta^{18}O$ values that are consistently higher than the contemporaneous river water and the $\delta^{18}O$–δ^2H relationship has a slope of 5.4, indicating evaporative influences (Table 4). The soil water isotope values generally reflect the seasonal patterns delineated by the river and precipitation water isotopes. The slope of the soil water line (i.e., δ^2H–$\delta^{18}O$ trend) is 7.4, indicating only minor evaporative influences.

We predicted stable isotope values and patterns that we would have observed if the soil carbonate formed only via pedogenesis and if pedogenic carbonate was mixed with detrital carbonate (Figs. 6–8). The mixing model between the stable isotope compositions of detrital and pedogenic carbonate can satisfactorily explain the observed $\delta^{13}C$, $\delta^{18}O$, and Δ_{47} data for all sample types if samples have pedogenic fractions of approximately

Table 2. Stable carbon and oxygen isotope data from carbonates in the Reserve.

Sample ID	Depth (cm)	Carbonate morphology	$\delta^{13}C_c$ ‰ VPDB[a]	$\delta^{18}O_c$ ‰ VPDB[a]
20EGSR-50	−50	rind	−3.2	−7.3
20EGSR-55-60	−55	rind	−3.2	−6.2
20EGSR-slope-60-1	−60	rind	−5.6	−8.0
20EGSR-slope-60-2	−60	rind	−4.9	−7.9
20EGSR-slope-70-75	−70	rind	−3.0	−7.4
20EGSR-slope-100-105	−100	rind	−5.7	−8.3
20EGSR-slope-120	−120	rind	−5.1	−8.0
22ESGR-whitestripe-200to220cm	−210	white matrix in bulk soil	−2.5	−6.6
22ESGR-rhizolith-180cm	−180	rhizolith	−7.2	−7.4
22ESGR-whitestripe-160to180cm	−170	white matrix in bulk soil	−6.6	−7.7
22ESGR-bulk-160to180cm	−170	homogenized bulk soil	−2.7	−8.2
22ESGR-bulk-120to140cm	−130	homogenized bulk soil	0.2	−6.2
22ESGR-whitestripe-80to100cm	−90	white matrix in bulk soil	−6.0	−7.7
22ESGR-bulk-80to100cm	−90	homogenized bulk soil	−2.3	−7.0
22ESGR-whitestripe-70to80cm	−75	white matrix in bulk soil	−3.6	−6.8
22ESGR-sand-rhizo-290cm	−290	rhizolith	−6.1	−6.4
22ESGR-sand-rhizo-270cm	−270	rhizolith	−7.9	−7.4
22ESGR-sand-bulk-300cm	−300	bulk sediment	−1.2	−6.2
22ESGR-lowergravel-325to375cm	−350	bulk sediment	−0.2	−5.4
20EGSR-100-105-lst-clast	−100	limestone clast	−0.4	−6.9
20ESGR-70-75-lst-clast	−70	limestone clast	2.5	−7.7

[a]$\delta^{13}C$ and $\delta^{18}O$ data are generated via CO_2 on a Kiel Device. Typical precision is ±0.1.

$0.6 \leq F \leq 1$ (Fig. 7). The calculated $\delta^{18}O_{rsw}$ values overlap with the highest observed $\delta^{18}O$ values of precipitation, river, marsh, and soil water isotope values (Fig. 5). The environmental conditions required to match the measured $\delta^{13}C_c$ have no or minimal overlap with modern conditions (Fig. 8). Only one rhizolith, with the lowest $\delta^{13}C$ value, could potentially be consistent with modern soil conditions.

Discussion

Physical evidence of pedogenic carbonate

The carbonate morphology and underlying sedimentology supports post-glacial pedogenic carbonate formation (Fig. 2). Our initial observations of carbonate morphology are strongly suggestive of in situ pedogenic carbonate precipitation (Gile et al., 1966; West et al., 1988b; Gocke and Kuzyakov, 2011; Zamanian et al., 2016) (Fig. 2). Calcite rinds indicate in situ recrystallization of calcite, though they are typically described in deserts (Gile et al., 1966). Rhizoliths cross cut sedimentary bedding structures and often surround roots of living plants. Filaments of calcite-rich material, called stringers, are also indicative of pedogenic processes. The diffuse carbonate in the matrix throughout the sedimentary sequence is equally likely to be finely ground detrital limestone or secondary carbonate (Kraimer and Monger, 2009; Li et al., 2013; Zamanian et al., 2021).

Table 3. Clumped isotope (Δ_{47}) data and calculated $\delta^{18}O_{rsw}$ values for select soil carbonates from the Reserve.

Sample ID	Num Δ_{47} analyses	Δ_{47} ICDES-90 ‰	Δ_{47} ERR[a]	TΔ_{47} °C	TΔ_{47} ERR	$\delta^{18}O_{rsw}$ ‰ SMOW	$\delta^{18}O_{rsw}$ ERR
20EGSR-50	5	0.593	0.007	25	2	−4.8	0.5
20EGSR-slope-70-75	4	0.572	0.007	33	3	−3.5	0.5
20EGSR-slope-120	4	0.604	0.007	22	3	−6.3	0.5
22ESGR-rhizolith-180cm	3	0.622	0.008	16	3	−6.9	0.5
20EGSR-100-105-lst-clast	2	0.486	0.010	70	5	3.4	0.8
20ESGR-70-75-lst-clast	3	0.456	0.008	87	5	5.1	0.7

[a]Δ_{47} ERR is calculated as the larger of 1 SD of sample measurements or 0.014 (the long term SD of in-house standard 102GCAZ01) divided by the square root of the number of measurements.

Table 4. Summary of meteoric and soil water isotope ($\delta^{18}O$, δ^2H) data.

Water type	Precipitation	River	Marsh	Soil
Slope	7.8	5.5	5.4	7.5
Intercept	11.8	−9.6	−8.2	3.5
r^2	0.98	0.91	0.95	0.90
Observations	160	167	12	29
Mean $\delta^{18}O$	−9.5	−7.3	−4.6	−6.6

Isotopic evidence for pedogenic carbonate and its formation processes

We examined the stable isotope data in the context of three scenarios to explain the origin of the soil carbonate: (1) a mixture of pedogenic and detrital carbonate; (2) pedogenic carbonate formed under equilibrium, open-system conditions; and (3) pedogenic carbonate formed in closed-system conditions (Fig. 6). Each of these scenarios would yield distinct isotope patterns (in $T\Delta_{47}$, $\delta^{18}O$, and $\delta^{13}C$) in the resulting soil carbonate (Fig. 6). The isotope and monitoring data are most consistent with the scenario that the soil carbonate is a mix between pedogenic and detrital carbonate.

A physical mixture of pedogenic and detrital carbonate

A mix between pedogenic and detrital endmembers can parsimoniously explain the observed isotopic values ($\delta^{18}O$, $\delta^{13}C$, $T\Delta_{47}$, and ^{14}C) of the carbonate (Figs. 6 and 7). Because the $\delta^{18}O$ value of the detrital limestone overlaps with the $\delta^{18}O$ value of pedogenic carbonate formed in equilibrium with modern waters, $\delta^{18}O$ is almost invariant in this scenario (Fig. 6), matching the measured $\delta^{18}O_c/\delta^{18}O_{rsw}$ values (Fig. 5). $T\Delta_{47}$ and $\delta^{13}C$ covary because both are dependent on the mixing fraction (Fig. 6). The detrital endmembers (limestone clasts) have high $T\Delta_{47}$ values of 70–86°C and high $\delta^{13}C$ values. The sampled rhizolith has a low $T\Delta_{47}$ of 16°C and a low $\delta^{13}C$ value, while the rinds have intermediate $T\Delta_{47}$ values of 21–33°C and intermediate $\delta^{13}C$ values (Fig. 6). Because of this variation, the $T\Delta_{47}$ values provide a strong constraint on the fraction of pedogenic carbonate within the samples ($0.5 \leq F \leq 1$) (Fig. 7). A mix between detrital and pedogenic carbonates is also consistent with the radiocarbon ages that predate glacial retreat; the radiocarbon-dead-detrital component would make ^{14}C ages appear older than their true formation age.

The distinctions in stable isotope values with carbonate morphology mostly fit with our expectation given a physical mix. The bulk samples have $\delta^{13}C$ and $\delta^{18}O$ values that overlap with that of the detrital limestone (Fig. 6 G and H, Table 2), which is expected given the higher potential for detrital contamination in bulk carbonate. For carbonate morphologies that are more likely to be composed of a higher proportion of pedogenic carbonate (rinds, rhizoliths, and stringers), the isotopic composition is explained via a mix of pedogenic and geogenic carbonate (Figs. 6 and 7). This framework groups rhizoliths, rinds, and stringers as having a higher proportion of pedogenic carbonate than bulk samples (Fig. 6), as also observed by Zamanian et al. (2021) and Gocke et al. (2011). Using this framework, the isotopic data suggest that the rhizoliths tend to have a higher proportion of pedogenic carbonate than rinds or stringers. This pattern could be a sampling artifact: The rinds were thin (∼1 mm) and

separating them from carbonate-cemented matrix was subjective. In comparison, the rhizoliths were more straightforward to isolate from matrix because they were thicker (∼1 cm), firm, had a predictable, cylindrical geometry, and were whiter than the surrounding matrix. This apparent difference in pedogenic component could be a true result that relates to their formation mechanisms. We might expect rinds to have matrix contamination if they form as hypocoatings in pore space that grow towards the clasts, rather forming gravitationally like a pedothem in arid soils (Ducloux et al., 1984; Durand et al., 2018). In comparison, rhizoliths have been previously shown to be purely secondary (pedogenic) carbonate (Gocke et al., 2011). In one model of rhizolith formation, the first step is that acidic root exudate dissolves the surrounding matrix (including detrital carbonate and noncarbonate minerals). Subsequently, the root selectively takes up Ca^{2+} in solution, then rhizolith carbonate precipitates from the remnant Ca^{2+} in solution and CO_2 from microorganism respiration (Barta, 2011; Brazier et al., 2020; Huguet et al., 2021). Therefore, the mixing model can explain the composition and origin of the soil carbonate at the Reserve.

The Monte Carlo mixing model gives predictions for the isotopic composition of the pedogenic carbonate endmembers (Fig. 7). The model predicts a range of $\delta^{13}C$ values for the pedogenic carbonate endmember, consistent with formation under mixed C_3–C_4 vegetation regimes or at substantially lower soil CO_2 concentrations than observed today. Our results are therefore consistent with, but do not uniquely identify, a substantial component of C_4 vegetation in southern Michigan in the late deglacial/Early Holocene (Nelson et al., 2006; Chapman and Brewer, 2008).

Alternative scenarios: pedogenic carbonate formed in modern open- or closed-system conditions

Given that the soil carbonate appears morphologically to be pedogenic, the simplest hypothesis is that the soil carbonate formed via pedogenic processes under post-glacial environmental conditions. However, the isotope data ($\delta^{18}O$, $\delta^{13}C$, $T\Delta_{47}$, and ^{14}C) and monitoring data are not fully compatible with this scenario (Figs. 5, 6, and 8).

The only evidence that aligns with the pedogenic carbonate scenario is that the $\delta^{18}O_{rsw}$ values overlap with the highest observed $\delta^{18}O$ values of precipitation, river, marsh, and soil water. These data could be consistent with pedogenic carbonate formation from parent soil waters during the warm half of the year (Fig. 5), but the other considered scenarios could also explain the measured $\delta^{18}O_c$ values (Fig. 6), so the information from $\delta^{18}O$ is nonunique at this site.

All other isotope data do not match our predictions for open-system, modern pedogenic carbonate. First, the radiocarbon ages of 17,366 and 23,691 cal yr BP predate glacial retreat from the region (Table 1) (Dalton et al., 2020), which would require pedogenic carbonate formation while the region was covered with an ice sheet. Second, the $T\Delta_{47}$ values of 16 to 33°C overlap or exceed the maximum measured soil temperatures (25°C) at 10 to 60 cm (Fig. 4). A simple interpretation of these data would suggest pedogenic carbonate formation during the warmest months (but even so, temperatures of 33°C are not reasonable). This interpretation is inconsistent with the $\delta^{13}C$ modeling that, in a C_3-dominated environment, requires formation at pCO$_2$ ∼<2500 ppm, and the fact that summer pCO$_2$ exceeds 8000 ppm. Finally, the $\delta^{13}C$ values of the soil carbonate samples are generally inconsistent with

predictions of values of pedogenic carbonate formed under modern conditions (colored dots in Fig. 8). The $\delta^{13}C$ values of most of the soil carbonate samples are higher than would be expected if they were pedogenic. The environmental conditions capable of recreating the measured soil carbonate $\delta^{13}C$ values are either low soil pCO_2 ($\sim<2500$ ppm) or $\delta^{13}C$ values of respired CO_2 of ~-20 to $-15‰$ (colored dots in Fig. 8). Neither of these conditions are consistent with modern conditions (black box in Fig. 7), where the minimum measured soil pCO_2 is 4000 ppm and the overlying vegetation is dominantly C_3 (forested) (measured $\delta^{13}C_{org}$ ranges from -29.4 to $-24.7‰$; Jin et al., 2009). The only samples for which there is some overlap in modeled and observed conditions are rhizoliths, which is consistent with stratigraphic evidence supporting that these are primarily modern (Figs. 6 and 8).

Another possibility is that the rind and bulk samples formed pedogenically immediately after glacial retreat, when the sparse vegetation coverage could lead to high $\delta^{13}C$–CO_2 values in the soil. This possibility could explain their relatively high $\delta^{13}C$ values (Fig. 8). However, it is difficult to explain why the post-glacial rinds would have higher formation temperatures than the modern rhizoliths (Tables 2 and 3, Fig. 6) given that post-glacial climates are cooler than the present day (c.f. varying seasonality of soil carbonate formation; Kelson et al., 2020). Furthermore, we might expect that the $\delta^{18}O$ of meteoric water and pedogenic carbonate would be different in post-glacial versus present-day southern Michigan, but we measured uniform $\delta^{18}O$ values amongst the sample types. The mixing model (scenario 1) is a simpler explanation that unifies all the data.

Theoretically, another possibility is that the soil carbonate is forming in situ, but rather than following the typical pedogenic model described above, the carbonate is re-precipitated from detrital carbonate in a closed system. Ultimately, this scenario is not consistent with the isotope and monitoring data (Fig. 6) and our understanding of shallow vadose zones. In a closed system, meteoric water equilibrates with the gas reservoir and dissolves pre-existing carbonate (i.e., detrital limestone) without further replenishment of CO_2 or water. Jin et al. (2009) reported that the vadose zone in the Reserve might be partially closed based on elevated values of $\delta^{13}C$ of dissolved inorganic carbon at depths >1.7 m, but those data could also represent equilibrium values at a high pH. A closed system would yield variable $\delta^{13}C$ values and invariant $\delta^{18}O$ values: The $\delta^{13}C$ of carbonate increases with cycles of dissolution and re-precipitation but the $\delta^{18}O$ of carbonate retains the $\delta^{18}O$ value derived from meteoric water (Salomons and Mook, 1986; Lohmann, 1988) (Fig. 6). This predicted $\delta^{18}O$ versus $\delta^{13}C$ pattern is displayed by the soil carbonates in the Reserve but could be explained by other scenarios (Fig. 6). Closed-system precipitation could also explain the "too-old" ^{14}C ages, whereby ^{14}C in the soil pore waters would be partially derived from dissolved limestone and/or pre-glacial, inherited organic matter (Wang et al., 1996). However, under closed-system precipitation we would expect uniform clumped isotope temperatures resembling mean annual air temperature at the depths of carbonate formation (>50 cm) (Quade et al., 2013; c.f. seasonal biases in Kelson et al., 2020) (Fig. 6). Instead, we document variation in $T\Delta_{47}$ that correlates with $\delta^{13}C$ (Fig. 6). Furthermore, under a closed or partially closed system, we might expect an increase in $\delta^{13}C$ with depth, where shallow carbonates form under a more open system. We do not find a depth–$\delta^{13}C$ pattern (Fig. 3), though this pattern may be difficult to detect given that we observe distinct carbonate morphologies with depth (i.e., the

deepest carbonates are rhizoliths, which are unlikely to be closed system given their adjacency to roots). Previous workers have shown open-system behavior at depths of $\sim<1$ m in soils: Even in limestone terrane, pedogenic $\delta^{13}C$ values match predictions of the pedogenic model of mixed atmospheric and respired CO_2 with a negligible contribution of CO_2 dissolved from parent limestone (Amundson et al., 1989; Cerling and Quade, 1993). Given these inconsistencies, pedogenic formation in a partially closed vadose zone is unlikely to be the dominant mode of carbonate formation at the Reserve.

Processes driving pedogenic carbonate formation in southern Michigan and implications for carbon cycling

We can confidently determine that pedogenic carbonate has formed in our field site in southern Michigan, even if it is physically mixed with detrital carbonate, and our data allow us to consider the process(es) driving its formation.

In arid settings, it is thought that pedogenic calcite precipitation is driven by wetting and drying cycles. Infiltrating precipitation dissolves Ca-bearing minerals and brings Ca^{2+} ions (e.g., from dust; Reheis, 2006) from the surface to depths in the soil profile. When the soil pore water dries via evapotranspiration, it reaches supersaturation with respect to calcite, and calcite precipitates (e.g., Breecker et al., 2009; Tabor et al., 2013; Gallagher and Sheldon, 2016; Huth et al., 2019; Kelson et al., 2023). However, soil drying is probably not the major mechanism driving pedogenic carbonate formation in the Reserve because (1) we observed little variation in soil water content, outside of minor increases after summer rain (Fig. 4), and (2) there is little isotopic evidence of evaporation in the soil waters (Fig. 5, Table 4). The $\delta^{18}O$–δ^2H composition of the soil waters falls near the local meteoric water line and has a slope of 7.5 (Table 4); typical soil water evaporation slopes in arid places are 2–3 (Benettin et al., 2018; Bowen et al., 2018). The isotopic composition of the soil waters reflects seasonal patterns of precipitation. For example, we observed wholesale isotope reset to the measured depths of 50 cm after precipitation events between September 3, 2021 and October 28, 2021, indicating significant infiltration of unevaporated soil water. In this setting, the formation of pedogenic carbonate is not controlled by a balance between incoming precipitation and soil drying. And, unlike desert settings where carbonate accumulates with time into progressively mature Bk horizons (Gile, 1961; Gile et al., 1966), soil carbonate may not be accumulating in the Reserve.

Instead, we propose that in the Reserve the pedogenic carbonate is forming ultimately because of an abundant supply of aqueous Ca^{2+} derived from glacially ground limestone and dolostone in the parent till and seasonal cycles in soil respired CO_2 (Jin et al., 2008a). Fine-grained carbonates, like those ground up by glaciers, are particularly susceptible to dissolution and recrystallization (Anderson et al., 1997; Gallagher and Breecker, 2020). We hypothesize that the detrital limestone is dissolving and re-repreicipating on a seasonal basis, resulting in pedogenic carbonate formation as an intermediate product (also described by West et al., 1988a). The $^{87}Sr/^{86}Sr$ values of ≈0.709 suggest that the source of Ca^{2+} is marine limestone (or dust derived from marine limestone). In the nearby Huron and Kalamazoo watersheds, Jin et al. (2008a) found that the saturation index of calcite in pore water is constant throughout the year, while the Ca^{2+} concentrations increased during the summer via calcite dissolution at higher pCO_2. In the surface water, lakes, and wetlands, however,

secondary calcite precipitates due to degassing (Szramek and Walter, 2004). Our data also show that pCO_2 increases in the summer, probably due to soil respiration. Put together, this evidence suggests that the in situ precipitation of pedogenic carbonate in the soil is driven by cycles of soil-respired pCO_2. Higher soil temperatures enable increased respiration, which increases soil pCO_2 and dissolves existing fine-grained calcite while maintaining a constant saturation index. Subsequently, cooling in the fall results in decreased respiration, decreased pCO_2, and decreased Ca^{2+} ions in the pore water as the calcite re-precipitates. This timing and mechanism are consistent with the stable isotope composition of the rhizolith sample that we hypothesize best represents the pedogenic endmember (i.e., the sample with the lowest $\delta^{13}C$ and $T\Delta_{47}$ values). The $T\Delta_{47}$ of the rhizolith is $16 \pm 3°C$, matching soil temperatures in September to October when pCO_2 is likely decreasing. Our observations support that soil respiration rates, which influence the acid-carrying capacity of soil pore waters, are an important lever in controlling the dissolution and re-precipitation of carbonate in the soil profile, and ultimately the export of bicarbonate to streams (Calmels et al., 2014; Romero-Mujalli et al., 2019).

Another factor contributing to pedogenic carbonate formation may be the mixed carbonate mineralogy in the watershed. Dolomite is less soluble and dissolves more slowly than calcite in the temperate climate of southern Michigan. Ground waters and surface waters in the Huron River watershed are undersaturated with respected to dolomite $(MgCa(CO_3)_2)$ but supersaturated with respect to calcite $(CaCO_3)$ (Williams et al., 2007; Jin et al., 2008b). Continued dissolution of dolomite (which releases Ca^{2+} and Mg^{2+}) after soil water is saturated with respect to calcite may contribute to calcite supersaturation in the watershed, setting the stage for calcite re-precipitation.

The pedogenic carbonate at the Reserve may represent a geologically transient feature. The carbonate has been leached from the top ~0.5 to 1.5 m at the Reserve after glacial retreat and at similar profiles described in the region (Figs. 2 and 3) (Jin et al., 2008a, 2009). There is net dissolution of carbonate minerals in the Huron River watershed (Williams et al., 2007; Jin et al., 2008b). It is likely that the observed pedogenic carbonate will ultimately be dissolved and carried away by ground water on geologic timescales. Thus, the morphology, depth, and amount of pedogenic carbonate in this profile are transient, adjusting to postglacial conditions. It is unlikely that such soil profiles with chemistry adjusting to changing climate conditions would be preserved in the geologic record as paleosols. If they were preserved, paleosols analogous to those currently found in the Reserve would be poor records of paleoclimate because the stable isotopic composition does not perfectly reflect environmental conditions in all samples. Even as a transient feature, the pedogenic carbonate represents an important intermediate step in watershed-scale carbonate weathering. The back-precipitation of carbonates in soils could help explain the missing Ca^{2+} in solute chemistry of rivers (Cavazza et al., 1993; Erlanger et al., 2021; Bufe et al., 2022) and could delay the export of bicarbonate from parent material to the ocean.

Conclusion

We presented physical and isotopic evidence for pedogenic carbonate formation in the humid, temperate climate of southern Michigan. The isotope values of the soil carbonate are most simply interpreted as a mixture of pedogenic and detrital carbonate. Because of the detrital component in this carbonate-rich glacial drift, paleoclimate reconstructions based on primary pedogenic carbonate material would require finer-scale techniques like laser ablation or secondary ion mass spectrometry (Passey and Cerling, 2006; Oerter et al., 2016; Huth et al., 2020). For hand-drilled samples, it is preferable to avoid limestone terranes when developing soil-based paleoclimate records (Kraimer and Monger, 2009; Sheldon and Tabor, 2009; Cotton and Sheldon, 2012; Michel et al., 2013).

The apparent in situ precipitation of rinds and rhizoliths has implications for terrestrial pools of inorganic carbon and carbon cycling. First, this study demonstrates the existence of pedogenic carbonate, at least transiently, in a wider range of ecosystems than is typically recognized (Railsback, 2021; Licht et al., 2022). Though there is net dissolution of carbonates in the glacial till in southern Michigan (Szramek and Walter, 2004), the timescale of dissolution is mediated by open-system re-precipitation of calcite in the shallow weathering zone, driven by seasonal fluctuations in soil respired CO_2. Because the formation of pedogenic calcite is likely driven by soil-respired CO_2, changes in land use and vegetation cover could affect the rates and amount of net calcite precipitation in this setting. Given that much of the Midwest is deeply mantled in glacial till that may also be rich in finely ground detrital carbonates, it is possible that re-reprecipitation of pedogenic carbonate may be occurring across much of the landscape. Our results raise the question of how the rates and magnitudes of this calcite re-precipitation mediate the net dissolution of parent limestone and dolomite and thus slow the export of dissolved bicarbonate. If back-precipitation as pedogenic carbonate is occurring on a sufficiently large scale, it could be relevant to considerations of post-glacial chemical weathering rates (Szramek and Walter, 2004), orogen-scale carbonate weathering rates (Erlanger et al., 2021; Bufe et al., 2022), and the efficacy of enhanced weathering in carbonate-rich till (Knapp and Tipper, 2022). Back-precipitation of detrital carbonate as pedogenic carbonate may alter the timing of regional carbon cycling, potentially acting to slow the glacial-enhancement of chemical weathering and attendant CO_2 sequestration that is a negative feedback on climate on medium ($\sim$thousand-year) timescales (Sharp et al., 1995; Anderson et al., 2000; Williams et al., 2007), even if it does not alter the geologically long-term ($\sim$million year) sequestration (Berner et al., 1983).

will be available at the University of Utah Water Isotope Database upon publication: https://wateriso.utah.edu/waterisotopes/index.html and in Supplementary Table S3.

References

Amundson, R.G., Chadwick, O.A., Sowers, J.M., Doner, H.E., 1988. Relationship between climate and vegetation and the stable carbon isotope chemistry of soils in the eastern Mojave Desert, Nevada. *Quaternary Research* **29**, 245–254.

Amundson, R.G., Chadwick, O.A., Sowers, J.M., Doner, H.E., 1989 The stable isotope chemistry of pedogenic carbonates at Kyle Canyon, Nevada. *Soil Science Society of America Journal* **53**, 201–210.

Anderson, N.T., Kelson, J.R., Kele, S., Daëron, M., Bonifacie, M., Horita, J., Mackey, T.J., et al., 2021. A unified clumped isotope thermometer calibration (0.5–1,100°C) using carbonate-based standardization. *Geophysical Research Letters* **48**, 1–11.

Anderson, S.P., Drever, J.I., Frost, C.D., Holden, P., 2000. Chemical weathering in the foreland of a retreating glacier. *Geochimica et Cosmochimica Acta* **64**, 1173–1189.

Anderson, S.P., Drever, J.I., Humphrey, N.F., 1997. Chemical weathering in glacial environments. *Geology* **25**, 399–402.

Arguez, A., Durre, I., Applequist, S., Vose, R.S., Squires, M.F., Yin, X., Heim, R.R., Owen T.W., 2012. NOAA's 1981–2010 U.S. climate normals: an overview. *Bulletin of the American Meteorological Society* **93**, 1687–1697.

Arkley, R.J., 1963. Calculation of carbonate and water movement in soil from climatic data. *Soil Science* **96**, 239–248.

Aron, P.G., Poulsen, C.J., Fiorella, R.P., Matheny, A.M., Veverica, T.J., 2020. An isotopic approach to partition evapotranspiration in a mixed deciduous forest. *Ecohydrology* **13**, 1–19.

Barta, G., 2011. Secondary carbonates in loess-paleosoil sequences: a general review. *Open Geosciences* **3**, 129–146.

Benettin, P., Volkmann, T.H.M., Von Freyberg, J., Frentress, J., Penna, D., Dawson, T.E., Kirchner, J.W., 2018. Effects of climatic seasonality on the isotopic composition of evaporating soil waters. *Hydrology and Earth System Sciences* **22**, 2881–2890.

Bereiter, B., Eggleston, S., Schmitt, J., Nehrbass-Ahles, C., Stocker, T.F., Fischer, H., Kipfstuhl, S., Chappellaz, J., 2015. Revision of the EPICA Dome C CO_2 record from 800 to 600 kyr before present. *Geophysical Research Letters* **42**, 542–549.

Bernasconi, S.M., Daëron, M., Bergmann, K.D., Bonifacie, M., Meckler, A.N., Affek, H.P., Bajnai, D., et al., 2021. InterCarb: a community effort to improve interlaboratory standardization of the carbonate clumped isotope thermometer using carbonate standards. *Geochemistry, Geophysics, Geosystems* **22**, e2020GC009588. https://doi.org/10.1029/2020GC009588

Berner, R.A., Lasaga, A.C., Garrels, R.M., 1983. The carbonate-silicate geochemical cycle and its effect on atmospheric carbon dioxide over the past 100 million years. *American Journal of Science* **283**, 641–683.

Birkeland, P.W., 1984. *Soils and Geomorphology.* Oxford University Press, New York.

Bowen, G.J., Putman, A., Brooks, J.R., Bowling, D.R., Oerter, E.J., Good, S.P., 2018. Inferring the source of evaporated waters using stable H and O isotopes. *Oecologia* **187**, 1025–1039.

Brand, W., Assonov, S.S., Coplen, T.B., 2010. Correction for the ^{17}O interference in $\delta(^{13}C)$ measurements when analyzing CO_2 with stable isotope mass spectrometry (IUPAC Technical Report). *Pure and Applied Chemistry* **82**, 1719–1733.

Brazier, J.-M., Schmitt, A.-D., Gangloff, S., Pelt, E., Gocke, M.I., Wiesenberg, G.L.B., 2020. Multi-isotope approach ($\delta^{44}/^{40}Ca$, $\delta^{88}/^{86}Sr$ and $^{87}Sr/^{86}Sr$) provides insights into rhizolith formation mechanisms in terrestrial sediments of Nussloch (Germany). *Chemical Geology* **545**, 119641. https://doi.org/10.1016/j.chemgeo.2020.119641

Breecker, D.O., Sharp, Z.D., McFadden, L.D., 2009. Seasonal bias in the formation and stable isotopic composition of pedogenic carbonate in modern soils from central New Mexico, USA. *Geological Society of America Bulletin* **121**, 630–640.

Bufe, A., Cook, K.L., Galy, A., Wittmann, H., Hovius, N., 2022. The effect of lithology on the relationship between denudation rate and chemical weathering pathways – evidence from the eastern Tibetan Plateau. *Earth Surface Dynamics* **10**, 513–530.

Calmels, D., Gaillardet, J., François, L., 2014. Sensitivity of carbonate weathering to soil CO_2 production by biological activity along a temperate climate transect. *Chemical Geology* **390**, 74–86.

Cavazza, W., Zuffa, G.G., Camporesi, C., Ferretti, C., 1993. Sedimentary recycling in a temperate climate drainage basin (Senio River, north-central Italy): composition of source rock, soil profiles, and fluvial deposits. In: Johnsson, M.J., Basu, A. (Eds.), *Processes Controlling the Composition of Clastic Sediments.* Geological Society of America Special Papers 284. Geological Society of America, Boulder, CO, pp. 247–262.

Cerling, T.E., 1984. The stable isotopic composition of modern soil carbonate and its relation to climate. *Earth Planetary Science Letters* **71**, 229–240.

Cerling, T.E., Quade, J., 1993. Stable carbon and oxygen isotopes in soil carbonates. *Geophysical Monograph* **78**, 217–231.

Chapman, K.A., Brewer, R., 2008. Prairie and savanna in southern Lower Michigan: history, classification, ecology. *The Michigan Botanist* **47**, 1–48.

Comer, P.J., Albert, D.A., Wells, H.A., Hart, B.L., Raab, J.B., Price, D.L., Kashian, D.M., Corner, R.A., 1995. *Michigan's Presettlement Vegetation, as Interpreted from the General Land Office Surveys 1816-1856.* Digital map. Michigan Natural Features Inventory, Lansing, MI.

Coplen, T.B., 2007. Calibration of the calcite–water oxygen-isotope geothermometer at Devils Hole, Nevada, a natural laboratory. *Geochimica et Cosmochimica Acta* **71**, 3948–3957.

Cotton, J.M., Sheldon, N.D., 2012. New constraints on using paleosols to reconstruct atmospheric pCO_2. *Geological Society of America Bulletin* **124**, 1411–1423.

Daëron, M., 2021. Full propagation of analytical uncertainties in Δ_{47} measurements. *Geochemistry, Geophysics, Geosystems* **22**, e2020GC009592. https://doi.org/10.1029/2020GC009592

Daëron, M., Blamart, D., Peral, M., Affek, H.P., 2016. Absolute isotopic abundance ratios and the accuracy of Δ_{47} measurements. *Chemical Geology* **442**, 83–96.

Dalton, A.S., Margold, M., Stokes, C.R., Tarasov, L, Dyke, A.S., Adams, R.S., Allard, S., et al., 2020. An updated radiocarbon-based ice margin chronology for the last deglaciation of the North American Ice Sheet Complex. *Quaternary Science Reviews* **234**, 106223. https://doi.org/10.1016/j.quascirev.2020.106223

D'Avello, T.P., Waltman, W.J., Waltman, S.W., Thompson, J.A., Brennan, J., 2019. Revisiting the Pedocal/Pedalfer boundary and Soil Moisture Regimes using the javaNewhall simulation model and PRISM data. *Geoderma* **353**, 125–132.

Davidson, G.R., 1995. The stable isotopic composition and measurement of carbon in soil CO_2. *Geochimica et Cosmochimica Acta* **59**, 2485–2489.

Ducloux, J., Butel, P., Dupuis, T., 1984. Microséquence minéralogique des carbonates de calcium dans une accumulation carbonatée sous galets calcaires, dans l'Ouest de la France. *Pédologie* **34**(2), 161–177.

Durand, N., Monger, H.C., Canti, M.G., Verrecchia, E.P., 2018. Calcium carbonate features. In: Stoops, G., Marcelino, V., Mees, F. (Eds.), *Interpretation of Micromorphological Features of Soils and Regoliths.* 2nd ed. Elsevier, Amsterdam, pp. 205–258.

Eggleston, S., Schmitt, J., Bereiter, B., Schneider, R., Fischer, H., 2016. Evolution of the stable carbon isotope composition of atmospheric CO_2 over the last glacial cycle. *Paleoceanography* **31**, 434–452.

Eiler, J.M., 2007. "Clumped-isotope" geochemistry—the study of naturally-occurring, multiply-substituted isotopologues. *Earth and Planetary Science Letters* **262**, 309–327.

Erlanger, E.D., Rugenstein, J.K.C., Bufe, A., Picotti, V., Willett, S.D., 2021. Controls on physical and chemical denudation in a mixed carbonate-siliciclastic orogen. *Journal of Geophysical Research: Earth Surface* **126**, e2021JF006064. https://doi.org/10.1029/2021JF006064

Eswaran, H., Reich, F.P., Kimble, J.M., Beinroth, F.H., Padamnabhan, E., Moncharoen, P., 2000. Global carbon stocks. In: Lal, R., Kimble, J.M., Eswaran, H., Stewart, B.A. (Eds.), *Global Climate Change and Pedogenic Carbonates.* CRC Press, Boca Raton, FL.

Farrand, W.R., Bell, D.R., 1982. Quaternary geology of Southern Michigan. In: *Geological Publication QG-01, Quaternary Geology of Michigan.* Michigan Department of Natural Resources, Lansing, MI.

Ferdush, J., Paul, V., 2021. A review on the possible factors influencing soil inorganic carbon under elevated CO_2. *Catena* **204**, 105434. https://doi.org/10.1016/j.catena.2021.105434

Gallagher, T.M., Breecker, D.O., 2020. The obscuring effects of calcite dissolution and formation on quantifying soil respiration. *Global Biogeochemical Cycles* **34**, e2020GB006584. https://doi.org/10.1029/2020GB006584

Gallagher, T.M., Sheldon, N.D., 2016. Combining soil water balance and clumped isotopes to understand the nature and timing of pedogenic carbonate formation. *Chemical Geology* **435**, 79–91.

Gile, L.H., 1961. A classification of ca horizons in soils of a desert region, Dona Ana County, New Mexico. *Soil Science Society of America Journal* **25**, 52–61.

Gile, L.H., Peterson, F.F., Grossman, R.B., 1966. Morphological and genetic sequences of carbonate accumulation in desert soils. *Soil Science* **101**, 347–360.

Gocke, M., Kuzyakov, Y., 2011. Effect of temperature and rhizosphere processes on pedogenic carbonate recrystallization: relevance for paleoenvironmental applications. *Geoderma* **166**, 57–65.

Gocke, M., Pustovoytov, K., Kühn, P., Wiesenberg, G.L.B., Löscher, M., Kuzyakov, Y., 2011. Carbonate rhizoliths in loess and their implications for paleoenvironmental reconstruction revealed by isotopic composition: $\delta^{13}C$, ^{14}C. *Chemical Geology* **283**, 251–260.

Gröning, M., Lutz, H.O., Roller-Lutz, Z., Kralik, M., Gourcy, L., Pöltenstein, L., 2012. A simple rain collector preventing water re-evaporation dedicated for $\delta^{18}O$ and δ^2H analysis of cumulative precipitation samples. *Journal of Hydrology* **448–449**, 195–200.

Huguet, A., Bernard, S., El Khatib, R., Gocke, M.I., Wiesenberg, G.L.B., Derenne, S., 2021. Multiple stages of plant root calcification deciphered by chemical and micromorphological analyses. *Geobiology* **19**, 75–86.

Huntington, K.W., Petersen, S.V., 2023. Frontiers of carbonate clumped isotope thermometry. *Annual Review of Earth and Planetary Sciences* **51**, 611–641.

Hutchings, J.A., Konecky, B.L., 2023. Optimization of a Picarro L2140-i cavity ring-down spectrometer for routine measurement of triple oxygen isotope ratios in meteoric waters. *Atmospheric Measurement Techniques* **16**, 1663–1682.

Huth, T.E., Cerling, T.E., Marchetti, D.W., Bowling, D.R., Ellwein, A.L., Passey, B.H., 2019. Seasonal bias in soil carbonate formation and its implications for interpreting high-resolution paleoarchives: evidence from southern Utah. *Journal of Geophysical Research: Biogeosciences* **124**, 616–632.

Huth, T.E., Cerling, T.E., Marchetti, D.W., Bowling, D.R., Ellwein, A.L., Passey, B.H., Fernandez, D.P., Valley, J.W., Orland, I.J., 2020. Laminated soil carbonate rinds as a paleoclimate archive of the Colorado Plateau. *Geochimica et Cosmochimica Acta* **282**, 227–244.

Jin, L., Hamilton, S.K., Walter, L.M., 2008a. Mineral weathering rates in glacial drift soils (SW Michigan, USA): new constraints from seasonal sampling of waters and gases at soil monoliths. *Chemical Geology* **249**, 129–154.

Jin, L., Ogrinc, N., Hamilton, S.K., Szramek, K., Kanduc, T., Walter, L.M., 2009. Inorganic carbon isotope systematics in soil profiles undergoing silicate and carbonate weathering (Southern Michigan, USA). *Chemical Geology* **264**, 139–153.

Jin, L., Williams, E.L., Szramek, K.J., Walter, L.M., Hamilton, S.K., 2008b. Silicate and carbonate mineral weathering in soil profiles developed on Pleistocene glacial drift (Michigan, USA): mass balances based on soil water geochemistry. *Geochimica et Cosmochimica Acta* **72**, 1027–1042.

Kelson, J.R., Huntington, K.W., Breecker, D.O., Burgener, L.K., Gallagher, T.M., Hoke, G.D., Petersen, S.V., 2020. A proxy for all seasons? A synthesis of clumped isotope data from Holocene soil carbonates. *Quaternary Science Reviews* **234**, 106259. https://doi.org/10.1016/j.quascirev.2020.106259

Kelson, J.R., Huth, T.E., Passey, B.H., Levin, N.E., Petersen, S.V., Ballato, P., Beverly, E.J., *et al.*, 2023. Triple oxygen isotope compositions of globally distributed soil carbonates record widespread evaporation of soil waters. *Geochimica et Cosmochimica Acta* **355**, 138–160.

Kim, S.T., O'Neil, J.R., 1997. Equilibrium and nonequilibrium oxygen isotope effects in synthetic carbonates. *Geochimica et Cosmochimica Acta* **61**, 3461–3475.

Knapp, W.J., Tipper, E.T., 2022. The efficacy of enhancing carbonate weathering for carbon dioxide sequestration. *Frontiers in Climate* **4**, 928215. https://doi.org/10.3389/fclim.2022.928215

Kraimer, R.A., Monger, H.C., 2009. Carbon isotopic subsets of soil carbonate—a particle size comparison of limestone and igneous parent materials. *Geoderma* **150**, 1–9.

Li, G., Chen, J., Chen, Y., 2013. Primary and secondary carbonate in Chinese loess discriminated by trace element composition. *Geochimica et Cosmochimica Acta* **103**, 26–35.

Licht, A., Kelson, J., Bergel, S., Schauer, A., Petersen, S.V., Capirala, A., Huntington, K.W., Dupont-Nivet, G., Win, Z., Aung, D.W., 2022. Dynamics of pedogenic carbonate growth in the tropical domain of Myanmar. *Geochemistry, Geophysics, Geosystems* **23**, e2021GC009929. https://doi.org/10.1029/2021GC009929

Lohmann, K.C., 1988. Geochemical patterns of meteoric diagenetic systems and their applications to studies of paleokarst. In: James, N.P., Choquette, P.W. (Eds.), *Paleokarst*. Springer New York, New York, pp. 58–80.

Michel, L.A., Driese, S.G., Nordt, L.C., Breecker, D.O., Labotka, D.M., Dworkin, S.I., 2013. Stable-isotope geochemistry of vertisols formed on marine limestone and implications for deep-time paleoenvironmental reconstructions. *Journal of Sedimentary Research* **83**, 300–308.

Milstein, R.L., 1987. *Bedrock Geology of Southern Michigan*. Michigan Department of Natural Resources, Lansing, MI.

Monger, H.C., Kraimer, R.A., Khresat, S., Cole, D.R., Wang, X., Wang, J., 2015. Sequestration of inorganic carbon in soil and groundwater. *Geology* **43**, 375–378.

Naorem, A., Jayaraman, S., Dalal, R.C., Patra, A., Rao, C.S., Lal, R., 2022. Soil inorganic carbon as a potential sink in carbon storage in dryland soils—a review. *Agriculture* **12**, 1256. https://doi.org/10.3390/agriculture12081256

Nelson, D.M., Hu, F.S., Grimm, E.C., Curry, B.B., Slate, J.E., 2006. The influence of aridity and fire on Holocene prairie communities in the Eastern Prairie Peninsula. *Ecology* **87**, 2523–2536.

Nyachoti, S., Jin, L., Tweedie, C.E., Ma, L., 2019. Insight into factors controlling formation rates of pedogenic carbonates: a combined geochemical and isotopic approach in dryland soils of the US Southwest. *Chemical Geology* **527**, 118503. https://doi.org/10.1016/j.chemgeo.2017.10.014

Oerter, E.J., Sharp, W.D., Oster, J.L., Ebeling, A., Valley, J.W., Kozdon, R., Orland, I.J., *et al.*, 2016. Pedothem carbonates reveal anomalous North American atmospheric circulation 70,000-55,000 years ago. *Proceedings of the National Academy of Sciences of the United States of America* **113**, 919–924.

Passey, B.H., Cerling, T.E., 2006. In situ stable isotope analysis ($\delta^{13}C$, $\delta^{18}O$) of very small teeth using laser ablation GC/IRMS. *Chemical Geology* **235**, 238–249.

Pelletier, E.M., 2020. Variability of Meteoric Water Isotopes in the Great Lakes Region. Undergraduate Honors thesis, University of Michigan, Ann Arbor, MI.

Pfeiffer, M., Padarian, J., Vega, M.P., 2023. Soil inorganic carbon distribution, stocks and environmental thresholds along a major climatic gradient. *Geoderma* **433**, 116449. https://doi.org/10.1016/j.geoderma.2023.116449

Plaza, C., Zaccone, C., Sawicka, K., Méndez, A.M., Tarquis, A., Gascó, G., Heuvelink, G.B.M., Schuur, E.A.G., Maestre, F.T., 2018. Soil resources and element stocks in drylands to face global issues. *Scientific Reports* **8**, 13788. https://doi.org/10.1038/s41598-018-32229-0

Putman, A.L., Fiorella, R.P., Bowen, G.J., Cai, Z., 2019. A global perspective on local meteoric water lines: meta-analytic insight into fundamental controls and practical constraints. *Water Resources Research* **55**, 6896–6910.

Quade, J., Eiler, J.M., Daëron, M., Achyuthan, H., 2013. The clumped isotope geothermometer in soil and paleosol carbonate. *Geochimica et Cosmochimica Acta* **105**, 92–107.

Railsback, L.B., 2021. Pedogenic carbonate nodules from a forested region of humid climate in central Tennessee, USA, and their implications for interpretation of C_3-C_4 relationships and seasonality of meteoric precipitation from carbon isotope ($\delta^{13}C$) data. *Catena* **200**, 105169. https://doi.org/10.1016/j.catena.2021.105169

Reheis, M.C., 2006. A 16-year record of eolian dust in Southern Nevada and California, USA: controls on dust generation and accumulation. *Journal of Arid Environments* **67**, 487–520.

Reimer, P.J., Baillie, M.G.L., Bard, E., Bayliss, A., Beck, J.W., Blackwell, P.G., Ramsey, C.B., *et al.*, 2009. IntCal09 and Marine09 radiocarbon age calibration curves, 0–50,000 years cal BP. *Radiocarbon* **51**, 1111–1150.

Retallack, G.J., 2005. Pedogenic carbonate proxies for amount and seasonality of precipitation in paleosols. *Geology* **33**, 333–336.

Rieck, R.L., 1976. The Glacial Geomorphology of an Interlobate Area in Southeast Michigan: Relationships Between Landforms, Sediments, and Bedrock. PhD thesis, Michigan State University, East Lansing, MI.

Roller, N.E.G., 1974. *Airphoto Mapping of Ecosystem Development on the Edwin S. George Reserve.* Master's thesis, University of Michigan, Ann Arbor, MI.

Romanek, C.S., Grossman, E.L., Morse, J.W., 1992. Carbon isotopic fractionation in synthetic aragonite and calcite: effects of temperature and precipitation rate. *Geochimica et Cosmochimica Acta* **56**, 419–430.

Romero-Mujalli, G., Hartmann, J., Börker, J., 2019. Temperature and CO_2 dependency of global carbonate weathering fluxes – implications for future carbonate weathering research. *Chemical Geology* **527**, 118874. https://doi.org/10.1016/j.chemgeo.2018.08.010

Royer, D.L., 1999. Depth to pedogenic carbonate horizon as a paleoprecipitation indicator? *Geology* **27**, 1123–1126.

Rozanski, K., Araguás-Araguás, L., Gonfiantini, R., 1993. Isotopic patterns in modern global precipitation. In: Swart, P.K., Lohmann, K.C., McKenzie, J., Savin, S. (Eds.), *Climate Change in Continental Isotopic Records*. American Geophysical Union Geophysical Monograph 78. American Geophysical Union, Washington, D.C., pp. 1–36.

Salomons, W., Mook, W.G., 1986. Isotope geochemistry of carbonates in the weathering zone. In: Fritz, P., Fonts, J. Ch. (Eds.), *Handbook of Environmental Isotope Geochemistry. Volume 2: The Terrestrial Environment*. Elsevier B.V., Amsterdam, pp. 239–269.

Schaetzl, R.J., 1992. Texture, mineralogy, and lamellae development in sandy soils in Michigan. *Soil Science Society of America Journal* **56**, 1538–1545.

Schaetzl, R.J., 2001. Late Pleistocene ice-flow directions and the age of glacial landscapes in northern Lower Michigan. *Physical Geography* **22**, 28–41.

Schauer, A.J., Kelson, J.R., Saenger, C., Huntington, K.W., 2016. Choice of ^{17}O correction affects clumped isotope (Δ_{47}) values of CO_2 measured with mass spectrometry. *Rapid Communications in Mass Spectrometry* **30**, 2607–2616.

Sharififar, A., Minasny, B., Arrouays, D., Boulonne, L., Chevallier, T., Van Deventer, P., Field, D.J., *et al.*, 2023. Soil inorganic carbon, the other and equally important soil carbon pool: distribution, controlling factors, and the impact of climate change. In: Sparks, D.L. (Ed.), *Advances in Agronomy* 178. Elsevier, Amsterdam, pp. 165–231.

Sharp, M., Tranter, M., Brown, G.H., Skidmore, M., 1995. Rates of chemical denudation and CO_2 drawdown in a glacier-covered alpine catchment. *Geology* **23**, 61–64.

Sheldon, N.D., Tabor, N.J., 2009. Quantitative paleoenvironmental and paleoclimatic reconstruction using paleosols. *Earth-Science Reviews* **95**, 1–52.

Slessarev, E.W., Lin, Y., Bingham, N.L., Johnson, J.E., Dai, Y., Schimel, J.P., Chadwick O.A., 2016. Water balance creates a threshold in soil pH at the global scale. *Nature* **540**, 567–569.

Stanbery, C.A., Pierce, J.L., Benner, S.G., Lohse, K., 2017. On the rocks: quantifying storage of inorganic soil carbon on gravels and determining pedon-scale variability. *Catena* **157**, 436–442.

Stanbery, C., Ghahremani, Z., Huber, D.P., Will, R., Benner, S.G., Glenn, N., Hanif, T., *et al.*, 2023. Controls on the presence and storage of soil inorganic carbon in a semi-arid watershed. *Catena* **225**, 106980. https://doi.org/10.1016/j.catena.2023.106980

Steiger, R.H., Jäger, E., 1977. Subcommission on geochronology: convention on the use of decay constants in geo- and cosmochronology. *Earth and Planetary Science Letters* **36**, 359–362.

Strong, G.E., Giles, J.R.A., Wright, V.P., 1992. A Holocene calcrete from North Yorkshire, England: implications for interpreting palaeoclimates using calcretes. *Sedimentology* **39**, 333–347.

Stuiver, M., Reimer, P.J., 1993. Extended ^{14}C data base and revised CALIB 3.0 ^{14}C age calibration program. *Radiocarbon* **35**, 215–230.

Szramek, K., Walter, L.M., 2004. Impact of carbonate precipitation on riverine inorganic carbon mass transport from a mid-continent, forested watershed. *Aquatic Geochemistry* **10**, 99–137.

Tabor, N.J., Myers, T.S., Gulbranson, E., Rasmussen, C., Sheldon, N.D., 2013. Carbon stable isotope composition of modern calcareous soil profiles in California: implications for CO_2 reconstructions from calcareous paleosols. In: Driese, S.G., Nordt, L.C. (Eds.), *New Frontiers in Paleopedology and Terrestrial Paleoclimatology: Paleosols and Soil Surface Analog Systems*. SEPM Special Publication 104. SEPM (Society for Sedimentary Geology), Tulsa, OK, pp. 17–34.

Tipple, B.J., Pagani, M., 2007. The early origins of terrestrial C_4 photosynthesis. *Annual Review of Earth and Planetary Sciences* **35**, 435–461.

United States Department of Agriculture, Natural Resources Conservation Service, 2022. *Land Resource Regions and Major Land Resource Areas of the United States, the Caribbean, and the Pacific Basin*. United States Department of Agriculture, Natural Resources Conservation Service.

Veizer, J., Ala, D., Azmy, K., Bruckschen, P., Buhl, D., Bruhn, F., Garden, G.A.F., *et al.*, 1999. $^{87}Sr/^{86}Sr$, $\delta^{13}C$ and $\delta^{18}O$ evolution of Phanerozoic seawater. *Chemical Geology* **161**, 59–88.

Wang, Y., Cerling, T.E., Effland, W.R., 1993. Stable isotope ratios of soil carbonate and soil organic matter as indicators of forest invasion of prairie near Ames, Iowa. *Oecologia* **95**, 365–369.

Wang, Y., McDonald, E.V., Amundson, R.G., McFadden, L.D., Chadwick, O.A., 1996. An isotopic study of soils in chronological sequences of alluvial deposits, Providence Mountains, California. *Geological Society of America Bulletin* **108**, 379–391.

Wani, O.A., Kumar, S.S., Hussain, N., Wani, A.I.A., Babu, S., Alam, P., Rashid, M., Popescu, S.M., Mansoor, S., 2023. Multi-scale processes influencing global carbon storage and land-carbon-climate nexus: a critical review. *Pedosphere* **33**, 250–267.

West, A.G., Patrickson, S.J., Ehleringer, J.R., 2006. Water extraction times for plant and soil materials used in stable isotope analysis. *Rapid Communications in Mass Spectrometry* **20**, 1317–1321.

West, L.T., Drees, L.R., Wilding, L.P., Rabenhorst, M.C., 1988a. Differentiation of pedogenic and lithogenic carbonate forms in Texas. *Geoderma* **43**, 271–287.

West, L.T., Wilding, L.P., Hallmark, C.T., 1988b. Calciustolls in Central Texas: II. genesis of calcic and petrocalcic horizons. *Soil Science Society of America Journal* **52**, 1731–1740.

White, J.H., Defliese, W.F., 2023. $\delta^{13}C$ and $\delta^{18}O$ heterogeneities in carbonates: nonlinear mixing in the application of dual-carbonate-clumped isotope thermometer. *Rapid Communications in Mass Spectrometry* **37**, e9627. https://doi.org/10.1002/rcm.9627

Williams, E.L., Szramek, K.J., Jin, L., Ku, T.C.W., Walter, L.M., 2007. The carbonate system geochemistry of shallow groundwater–surface water systems in temperate glaciated watersheds (Michigan, USA): significance of open-system dolomite weathering. *Geological Society of America Bulletin* **119**, 515–528.

Zamanian, K., Lechler, A.R., Schauer, A.J., Kuzyakov, Y., Huntington, K.W., 2021. The $\delta^{13}C$, $\delta^{18}O$ and Δ_{47} records in biogenic, pedogenic and geogenic carbonate types from paleosol-loess sequence and their paleoenvironmental meaning. *Quaternary Research* **101**, 256–272.

Zamanian, K., Pustovoytov, K., Kuzyakov, Y., 2016. Pedogenic carbonates: forms and formation processes. *Earth-Science Reviews* **157**, 1–17.

Zhou, J., Chafetz, H.S., 2010. Pedogenic carbonates in Texas: stable-isotope distributions and their implications for reconstructing region-wide paleoenvironments. *Journal of Sedimentary Research* **80**, 137–150.